Nuclear Physics B267 (1986) 625–678

SUPERSYMMETRY – LOST OR FOUND?*

R.M. BARNETT

Lawrence Berkeley Laboratory, University of California, Berkeley, California 94720, USA

H.E. HABER

Division of Natural Sciences II, University of California, Santa Cruz, California 95064, USA and Stanford Linear Accelerator Center, Stanford University, Stanford, California 94305, USA

G.L. KANE

Randall Laboratory of Physics, University of Michigan, Ann Arbor, Michigan 48109, USA

Received 2 October 1985

We present a comprehensive analysis of missing transverse-energy events at the CERN $p\bar{p}$ collider which would arise from a supersymmetric theory. This analysis takes into account, the new 1984 UA1 cuts, triggers and resolutions. Our conclusions from the newly reported 1984 data are that any excess number of monojet events is highly unlikely to come from gluino or scalar quark production. The new data lead to the very restrictive limits: $M(\tilde{g})$ and $M(\tilde{q}) > 60$–70 GeV. The two intriguing dijet events with $E_T(\text{missing}) > 55$ GeV are not inconsistent with an 80 GeV gluino or scalar quark source. The above conclusions have been obtained assuming that photinos are lighter than gluinos and live long enough to escape collider detectors. An alternative picture where the higgsino is the lightest supersymmetric particle is briefly discussed.

1. Introduction

Nearly all experimental data which are available at present support the standard model as being the correct description of observable physics at current energies. The recent discoveries of the W and Z bosons exhibit all the properties [1] expected in the standard model. Nevertheless, theorists expect that the standard model is incomplete, and that new phenomena will emerge in the energy region below 1 TeV. Although the reasons for this are familiar, we briefly summarize them. The underlying physics of electroweak-symmetry breaking is not understood, nor is there any

* This work was supported by the Director, Office of Energy Research, Office of High Energy and Nuclear Physics, Division of High Energy Physics of the US Department of Energy under contract nos. DE-AC03-76SF00098, DE-AC02-76-01112, DE-AM03-76SF00010 and DE-AC03-76SF00515, and the US National Science Foundation under agreement no. PHY83-18358.

insight into why the weak scale is where it is, or how it can be so small compared to the Planck scale or the grand unification scale [2]. Models which try to understand these problems invariably lead to additional new physics around the weak scale.

Supersymmetry is an approach which many workers feel could help to explain these problems [3]. In this paper, we investigate phenomenological implications of assuming a supersymmetric explanation for the origin of electroweak symmetry breaking [4–8].

Under the assumption just stated, it is still not clear at what precise mass scale supersymmetric phenomena will appear. Roughly, one would expect supersymmetric masses to be of order m_W. If this is indeed the case, then supersymmetric particles would (perhaps) first be detectable at the Tevatron. However, without any firm predictions for supersymmetric masses, we must consider the possibilities that supersymmetric particles could be somewhat lighter or heavier than m_W. In the latter case, one would have to wait for a supercollider in order to discover supersymmetry [9]. In the former case, supersymmetry could be observable at accelerators now in operation. The most likely place of the present facilities to discover supersymmetry or provide the best possible supersymmetric mass limits is the CERN Collider.

Some time ago it was realized that hadron colliders were an excellent place to search for evidence for supersymmetry [10–13]. As we will see below, in an ideal detector the production of the supersymmetric partners of quarks and gluons gives events with signatures of jet + missing transverse energy, E_T^{miss} (monojets), 2 jets + E_T^{miss} (dijets), 3 or more jets + E_T^{miss} at various rates. The constituent cross sections for the production of superpartners of mass $\tilde{M}$ are order $\alpha_s^2/\tilde{M}^2 \approx$ few nb, so with an integrated luminosity of 100 nb^{-1}, even with an order of magnitude suppression due to hadronic structure effects, there would be a significant number of events expected until phase space cuts off the rate at masses above 60 GeV or so.

In early 1984, the analysis of data from the 1983 run at the CERN $\bar{p}p$ Collider (at $\sqrt{s} = 540$ GeV) by the UA1 collaboration [14] resulted in the report of candidates for events which seemed to be unexplainable by the standard model. These events were precisely of the type described above – events with jets and missing transverse momentum. This led to a plethora of papers attempting to explain these events as being evidence for new physics. By far the most popular explanation [15–22] was in terms of the production of supersymmetric particles – either scalar-quarks or gluinos. In the fall of 1984, more data was taken at a slightly higher energy, $\sqrt{s} = 630$ GeV. More than twice the luminosity (as compared to the 1983 run) was collected. It seems clear from the reports on the 1984 data [23] that the missing-energy events which are seen are (for the most part) less dramatic and possibly entirely explained by standard model backgrounds. Thus, the enthusiasm for the possible discovery of supersymmetry at CERN has certainly been dampened. On the other hand, our analysis of the 1984 data will provide much more stringent limits on supersymmetric particle masses.

Qualitatively, it is clear that significant numbers of supersymmetric particles can be produced at the CERN Collider if their masses are not too large. In this paper we describe a lengthy analysis to systematically calculate the quantitative predictions of supersymmetry for all scalar-quark ($\tilde{q}$) and gluino ($\tilde{g}$) masses. As will be discussed in detail below, a "theory" event of, say, $\tilde{g}\tilde{g}$ production will contain four quark jets plus missing momentum. However, some of the jets may be below the experimental definition of a jet, one with $E_T > 12$ GeV. Also, two of the jets may overlap to give one in the detector.

Why can supersymmetric processes lead to "monojets" (as opposed to multi-jet events)? The explanation comes entirely from the experimental cuts and triggers (as first pointed out by Ellis and Kowalski [15]). Consider one of the most difficult mechanisms for producing monojets: gluino pair production for light gluinos. Gluinos at rest would produce little missing energy. The experimental requirement that E_T^{miss} be large therefore implies that the gluinos must be sufficiently energetic, and for one of the gluinos, the photino from its decay must carry a large fraction of the gluino's momentum (we assume that photinos leave the apparatus undetected). Similarly the photino from the decay of the gluino going in the opposite direction must carry very little of this gluino's momentum (otherwise the two vectors would cancel). For this latter gluino the quarks from its decay carry much momentum, and their resultant jets are likely to coalesce (if they do not, then they are unlikely to pass the trigger requirements for leading jets). For the first gluino, little energy is left for the jets since the photino had to be very hard, and they are unlikely to have sufficient energy to be called a jet. While very few $\tilde{g}\tilde{g}$ pairs for light gluinos can pass the cuts, those that do pass turn out to have one rather than two or more jets.

On the other hand for heavy gluinos and scalar quarks, one finds that dijets dominate over monojets. In general a number of supersymmetric mechanisms must be computed, and complicated trigger biases and cuts must be imposed. Analytic calculations are not possible; a Monte Carlo procedure is required.

The plan of the paper is as follows. In sect. 2 we discuss some general features of supersymmetric models which are relevant for our analysis. In sect. 3, we review the parton model formalism which serves as a basis for all our predictions. Two related issues are discussed – the importance of hard gluon bremsstrahlung and the intrinsic gluino content of the proton. Both these issues are particularly relevant if the gluino is "light" (e.g. $M_{\tilde{g}} \leqslant 10$–$20$ GeV). The Monte Carlo procedure is discussed in detail in sect. 4. This is a procedure which results in the generation of "events," i.e., four-momenta of final state partons (which are treated as "jets") and photinos (which are the origin of the missing transverse energy). The most difficult part of the analysis is the modeling of the UA1 triggers and cuts, which is described in sect. 5. We have endeavored to reproduce those cuts and triggers which were used in the 1984 run; these differ somewhat from those used in the 1983 run. In sect. 6 we discuss the sensitivity of our results to these experimental conditions. Putting together the Monte Carlo event generator and the appropriate cuts and triggers, we

are able to make predictions for the expected number of missing transverse energy events and their distributions, as a function of the unknown supersymmetric particle masses. By comparing these results with the 1984 data as reported by the UA1 Collaboration, we extract limits for scalar-quark and gluino masses in sect. 7. We are able to rule out the existence of a "light" gluino, and we find that scalar-quark and gluino masses must be larger than 60–70 GeV. Considerable attention is given to the various uncertainties of the analysis and the "confidence" of our final limits. Sect. 8 discusses our limits in the context of the minimal low-energy supergravity approach. We also discuss the implications of the assumption that the higgsino rather than the photino is the lightest supersymmetric particle. Lastly, a discussion of future tests and our conclusions are presented in sect. 9.

2. Low energy supersymmetry

2.1. THE SUPERSYMMETRIC SPECTRUM AND ITS INTERACTIONS

It is easy to explain what would be observed if supersymmetric partners were to exist [4–7]. The minimal spectrum of a supersymmetric theory associates with each quark, lepton, gauge boson, and Higgs boson, a partner which differs by $\frac{1}{2}$ unit of spin. If the symmetry were unbroken there would be a particle identical to the electron but with spin zero (scalar-electron), a particle identical to the photon but with spin-$\frac{1}{2}$ (photino), etc. Such states would have been observed so either there is no such symmetry in nature, or the symmetry is broken and the missing partners have acquired extra mass.

The full spectrum includes scalar quarks ($\tilde{q}$), one for each flavor of quark (in addition the partners of left-handed quarks ($\tilde{q}_L$) and right-handed quarks ($\tilde{q}_R$) are kept separate since they have different weak interactions), scalar leptons ($\tilde{\ell}$), scalar neutrinos ($\tilde{\nu}$), gluinos ($\tilde{g}$), winos ($\tilde{w}$), zinos ($\tilde{z}$), and higgsinos ($\tilde{h}$). Spontaneous symmetry breaking mixes weak interaction eigenstates in forming mass eigenstates so considerable care is needed to get rates correct quantitatively.

Although the masses of superpartners must be treated as unknown parameters because the breaking of supersymmetry is not understood, all of the relevant coupling are known because they are the measured gauge couplings. In a supersymmetric theory, for every standard model vertex there also occur new vertices with the particles replaced in pairs by their superpartners, and the same coupling. Thus the $\bar{q}qg$ vertex generates $\bar{\tilde{q}}\tilde{q}g$ and $\bar{q}\tilde{q}\tilde{g}$ vertices all with strength g_s ($\alpha_s = g_s^2/4\pi$), the $We\nu$ vertex generates $\tilde{w}\tilde{e}\nu$, $\tilde{w}e\tilde{\nu}$, and $W\tilde{e}\tilde{\nu}$ vertices all with strength g_2 ($\alpha_2 = \alpha/\sin^2\theta_W = g_2^2/4\pi$), and the electromagnetic vertices $\gamma f\bar{f}$ for any fermion f generate $\tilde{\gamma}\tilde{f}\bar{f}$ and $\gamma\bar{\tilde{f}}\tilde{f}$ vertices of strength e ($e^2/4\pi = \alpha$). Following this rule one can draw Feynman diagrams for all supersymmetric production and decay processes and estimate rates. Detailed discussions of the spectrum, mixing, Feynman rules, calcula-

tional techniques, and possible ways to observe superpartners are given in the review article of ref. [6].

The unknown parameters in the supersymmetric model are masses and mixing angles. Thus, in any analysis, some assumptions will have to be made regarding these parameters. In this paper, we are concerned with processes involving the production of scalar-quarks and gluinos. To simplify our analysis, we assume that five flavors of scalar-quarks are degenerate in mass (we exclude the $\tilde{t}$ from the discussion). Furthermore, for each flavor, we assume that $\tilde{q}_L$ and $\tilde{q}_R$ are equal in mass. These assumptions are approximately true in almost all supersymmetry models which attempt to predict the supersymmetric mass spectrum. The only other major assumption we make is that the photino is the lightest supersymmetric particle. We will comment in more detail on this assumption in subsect. 2.3.

2.2. R-PARITY AND ITS CONSEQUENCES

An important feature of nearly all supersymmetric models is the existence of a conserved multiplicative quantum number called R-parity [24]. Specifically, for a particle with baryon number B, lepton number L and spin J, we define $R = (-1)^{3B+L+2J}$. It is easy to see that all "ordinary" particles have $R = +1$, whereas all supersymmetric partners have $R = -1$. This has some important consequences, First, if we start from an initial state consisting only of ordinary particles, supersymmetric particles must be produced in pairs. Second, there exists a lightest supersymmetric particle (i.e., the lightest $R = -1$ particle) which must be stable. Let us denote this particle by LSP. Once a superpartner is produced, it will decay into a normal ($R = 1$) particle plus a lighter superpartner. Eventually, at the end of a decay chain, one will find normal particles plus an odd number of LSPs. The LSP can be the partner of a gauge boson, a Higgs boson or a neutrino. In all cases, its essential property is that it normally escapes collider detectors [25]. That is because to interact it must excite a superpartner in the detector, and the partners of quarks and leptons are heavy, so the interaction cross section is at most of order $\alpha^2/\tilde{M}^2$ with $M \gtrsim 20$ GeV, giving too small a cross section to see.

Thus the basic signature of the production of supersymmetric partners is missing momentum, accompanied by jets (or occasionally charged leptons, if e.g., winos are produced) in characteristic patterns.

2.3. THE STANDARD ASSUMPTION: THE PHOTINO AS LSP

The question of the LSP in supersymmetric theories is a model dependent question. In principle, one must know the neutralino (neutral gaugino and higgsino) mass matrix. By diagonalizing, one obtains the LSP which may be some linear combination of photino, zino and higgsino [26]. In this paper, we shall assume that the LSP is the photino. This is relevant for the signatures of scalar-quarks and gluinos. For definiteness, let us suppose for the moment that $M_{\tilde{g}} > M_{\tilde{q}}$. If the $\tilde{\gamma}$ is

the LSP, then once scalar-quarks and gluinos are produced, they will decay via $\tilde{q} \to q\tilde{\gamma}$ and $\tilde{g} \to \bar{q}\tilde{q} \to q\bar{q}\tilde{\gamma}$. The photino escapes and is interpreted as missing energy. There are two alternative possibilities. First, the LSP is not a pure photino, but it is a mixture of photino and other neutralino states. The only changes which occur are minor – some decay rates are changed due to the appearance of mixing angle factors. As long as the mixing angles are not unusually small, all the results we obtain in this paper are basically unchanged. The second possibility is that the photino is not the LSP. This may or may not dramatically change our results depending on how the photino decays. For example, if the scalar-neutrino is the LSP, then $\tilde{\gamma} \to \nu + \tilde{\nu}$. But, both the ν and $\tilde{\nu}$ will not be observed, so the phenomenology will be identical to the case where the $\tilde{\gamma}$ is the LSP. On the other hand, if the LSP is a higgsino $\tilde{H}$, the phenomenology can be vastly different. As discussed in refs. [27–28], the $\tilde{\gamma}$ would decay dominantly via $\tilde{\gamma} \to \gamma + \tilde{H}$ thereby softening considerably the missing transverse energy of the events. (A similar affect arises if R-parity is broken [29, 30]. Then the $\tilde{\gamma}$ is unstable and decays via $\tilde{\gamma} \to \gamma + \nu$ leading to similar conclusions.) We will briefly consider the implications of this alternative scenario at the end of this paper (see sect. 8). Otherwise, all the analysis we present here will assume that the $\tilde{\gamma}$ is the LSP.

The mass of the photino is a priori an unknown parameter. In some supersymmetry models, the $\tilde{\gamma}$ and $\tilde{g}$ masses are related via [31].

$$\frac{M_{\tilde{\gamma}}}{M_{\tilde{g}}} = \frac{8}{3}\frac{\alpha}{\alpha_s} \approx \frac{1}{6}. \tag{2.1}$$

In all the calculations presented in this paper, we have taken $M_{\tilde{\gamma}} = 0$. Although this is not likely to be true, our results are not especially sensitive to the precise value of the photino mass, assuming that $M_{\tilde{\gamma}} \leqslant 10$ GeV. We will make a few comments on the implications of a photino mass in sect. 7.

3. Parton model formalism

3.1. THE BASICS

In order to predict the cross-section for the production of supersymmetric particles, the "QCD-improved" parton model is used. The basic formulas are summarized below. The starting point is:

$$\sigma(p\bar{p} \to c_1 + c_2 + X)$$

$$= \sum_{a,b} \int dx_1\, dx_2\, f_a^p(x_1, Q^2) f_b^{\bar{p}}(x_2, Q^2) \hat{\sigma}(\hat{s}, \hat{t}, \hat{u})^{a+b \to c_1 + c_2 + \cdots}, \tag{3.1}$$

where the sum is taken over all subprocesses which lead to the production of

particles $c_1, c_2, \ldots$ in the final state. We denote the partonic squared center of mass energy by $\hat{s} = x_1 x_2 s$ and the total integrated cross section for $a + b \to c_1 + c_2 + \cdots$ by $\hat{\sigma}$. The structure functions $f_a^{\mathrm{p}}(x, Q^2)$ represent the probability of finding initial parton a inside a proton p, etc. By "QCD-improved," we simply mean that scale-breaking structure functions are used and $\hat{\sigma}$ is computed as a function of the running coupling constant $\alpha_s(Q^2)$. The choice of Q^2 is ambiguous as long as we neglect higher order perturbative effects. We have chosen $Q^2 = \hat{s}$. We follow Eichten, et al. (EHLQ) [9] by using their structure functions and definition of α_s.

In order to improve convergence in the numerical integration, we make the following change of variables:

$$w = \frac{1}{x_1 x_2}, \tag{3.2}$$

$$y = \tfrac{1}{2} \log \frac{x_1}{x_2}. \tag{3.3}$$

Then,

$$\begin{aligned} &\sigma(\mathrm{p\bar{p}} \to c_1 + c_2 + \cdots \mathrm{X}) \\ &= \sum_{a,b} \int_1^{w_0} \frac{\mathrm{d}w}{w^2} \int_{-\frac{1}{2}\log w}^{\frac{1}{2}\log w} \mathrm{d}y f_a^{\mathrm{p}}(w^{-1/2} \mathrm{e}^{y}, Q^2) f_b^{\bar{\mathrm{p}}}(w^{-1/2} \mathrm{e}^{-y}, Q^2) \\ &\quad \times \hat{\sigma}(\hat{s}, \hat{t}, \hat{u})^{a+b \to c_1 + c_2 + \cdots}, \end{aligned} \tag{3.4}$$

where $w_0 = s/s_{\min}$, where $s_{\min}$ is the threshold value of $\hat{s}$ for the reaction of interest.

Let us now concentrate on how to compute $\hat{\sigma}$. We write

$$\hat{\sigma} = \frac{1}{2s} (2\pi)^{4-3n} \frac{1}{F_{\mathrm{I}}} \int \prod_{i=1}^{n} \frac{\mathrm{d}^3 p_i}{(2\pi)^3 (2E_i)} |\tilde{\mathfrak{M}}|^2_{\mathrm{ave}}, \tag{3.5}$$

where $|\tilde{\mathfrak{M}}|^2_{\mathrm{ave}}$ is the squared amplitude for the process $a + b \to c_1 + c_2 + \cdots + c_n$, summed over final-state spins and colors, and averaged over initial spins and colors. The factor F_{I} is required if there are identical particles in the final state (e.g., $F_{\mathrm{I}} = 2$ for $\mathrm{gg} \to \tilde{\mathrm{g}}\tilde{\mathrm{g}}$, $\mathrm{gg} \to \tilde{\mathrm{g}}\tilde{\mathrm{g}}\mathrm{g}$, etc.). The amplitude depends on the outgoing momenta $p_1, \ldots, p_n$ as well as the two incoming momenta p_a and p_b given by:

$$p_a = \left(\tfrac{1}{2} x_1 \sqrt{s}\,; 0, 0, \tfrac{1}{2} x_1 \sqrt{s}\right), \tag{3.6a}$$

$$p_b = \left(\tfrac{1}{2} x_2 \sqrt{s}\,; 0, 0, \tfrac{1}{2} - x_2 \sqrt{s}\right). \tag{3.6b}$$

Inserting eq. (3.5) into eq. (3.4), we see that the computation of σ involves the

integration over w, y and final state four-momenta p_i. Furthermore, one may obtain any desired final-state distribution by restricting the integration over the p_i in the appropriate way. This is most easily done using Monte Carlo techniques which are discussed in detail in sect. 4.

The final necessary ingredient is an expression for $|\tilde{\mathcal{M}}|^2$ for each possible process $a + b \to c_1 + c_2 + \cdots + c_n$. The subprocess arises from the production of primary partons which then may decay into subsequent partons. After all decay chains are complete, the resulting final state is $c_1 + c_2 + \cdots + c_n$. The calculation of the squared amplitude under the most general circumstances is quite tedious since it requires the computation of spin-density matrices in order to correctly account for all final-state spin correlations. However, tremendous simplification occurs if we make two assumptions which are valid here. First, where intermediate states can be taken to be on-shell, they may be treated to good approximation in the narrow-width approximation. Second, all interactions involved in the decay chain separately conserve parity and *CP*. In this case, the production and decay amplitudes factorize. Actually, this is an artifact of the Born approximation, where all amplitudes are real. The argument is simple: first, the reality of the amplitudes imply that the outgoing particles (which decay) are not transversely polarized. Second, parity conservation implies that the outgoing particles are not longitudinally polarized. Hence, the production and decay density matrices are diagonal, implying factorization of the production and decay processes.

Let us illustrate that procedure in the case of $q\bar{q} \to \tilde{g}\tilde{\gamma}$, with $\tilde{g} \to q\bar{q}\tilde{\gamma}$. First, we denote the squared matrix element averaged over initial-state spins and summed over final-state spins and colors by $|\tilde{\mathcal{M}}|^2_{\text{ave}}$. The squared matrix elements for $q\bar{q} \to \tilde{g}\tilde{\gamma}$ is given by eq. (A.21) and for $\tilde{g} \to q\bar{q}\tilde{\gamma}$ by eq. (A.23). It then follows that, in the narrow-width approximation for the gluino decay (taking the gluino on-shell), the squared amplitude for the process $q\bar{q} \to q\bar{q}\tilde{\gamma}\tilde{\gamma}$ via $\tilde{g}\tilde{\gamma}$ production summed and averaged over spins and colors is:

$$|\tilde{\mathcal{M}}(q\bar{q} \to q\bar{q}\tilde{\gamma}\tilde{\gamma})|^2_{\text{ave}}$$

$$= |\tilde{\mathcal{M}}(q\bar{q} \to \tilde{g}\tilde{\gamma})|^2_{\text{ave}} |\tilde{\mathcal{M}}(\tilde{g} \to q\bar{q}\tilde{\gamma})|^2_{\text{ave}} \frac{\pi}{M_{\tilde{g}}\Gamma_{\tilde{g}}} \delta\left(M^2_{\tilde{g}} - (p_1 + p_2 + p_3)^2\right). \quad (3.7)$$

It is this matrix element which we insert into eq. (3.5).

A small technical note may be of interest here. In general, one must consider the diagram with the two final-state photino lines crossed. In addition, one must insert a factor of $\frac{1}{2}$ for the identical photinos in the final state. However, in the narrow-width approximation, in the limit that the gluino is exactly on-shell, the interference term between the original $q\bar{q} \to q\bar{q}\tilde{\gamma}\tilde{\gamma}$ amplitude and the crossed amplitude vanishes (it is actually proportional to the gluino width). Thus, in computing the total cross section, one obtains identical results whether one treats the two final state photinos

as being identical (following the above procedure), or as being non-identical (in which case no crossed graph need be considered).

To summarize, given a partonic subprocess $a + b \to x + y + \cdots$ with $x \to c_1 + c_2 + \cdots$, $y \to c_3 + c_4 + \cdots$, we compute:

$$
\begin{aligned}
&|\tilde{\mathfrak{M}}(a + b \to c_1 + c_2 + \cdots + c_n)|^2_{\text{ave}} \\
&\quad = |\tilde{\mathfrak{M}}(a + b \to x + y + \cdots)|^2_{\text{ave}} \\
&\qquad \times |\tilde{\mathfrak{M}}(x \to c_1 + c_2 + \cdots)|^2_{\text{ave}} \times |\tilde{\mathfrak{M}}(y \to c_3 + c_4 + \cdots)|^2_{\text{ave}} \\
&\qquad \times \frac{\pi}{M_x \Gamma_x} \delta\left(M_x^2 - (p_1 + p_2 + \cdots)^2\right) \frac{\pi}{M_y \Gamma_y} \delta\left(M_y^2 - (p_3 + p_4 - \cdots)^2\right),
\end{aligned}
\tag{3.8}
$$

which is then inserted into eq. (3.3). In this paper, we shall consider the following possible subprocesses: First, we list the production processes:

(i) Gluino pair production

$$\mathrm{gg} \to \tilde{\mathrm{g}}\tilde{\mathrm{g}}, \tag{3.9a}$$

$$\mathrm{q\bar{q}} \to \tilde{\mathrm{g}}\tilde{\mathrm{g}}. \tag{3.9b}$$

(ii) Scalar-quark pair production

$$\mathrm{gg} \to \tilde{\mathrm{q}}\bar{\tilde{\mathrm{q}}}, \tag{3.10a}$$

$$\mathrm{q\bar{q}} \to \tilde{\mathrm{q}}\bar{\tilde{\mathrm{q}}}, \tag{3.10b}$$

$$\mathrm{qq} \to \tilde{\mathrm{q}}\tilde{\mathrm{q}}, \tag{3.10c}$$

$$\mathrm{q\bar{q}} \to \mathrm{W} \to \tilde{\mathrm{q}}\bar{\tilde{\mathrm{q}}}, \tag{3.11a}$$

$$\mathrm{q\bar{q}} \to \mathrm{Z} \to \tilde{\mathrm{q}}\bar{\tilde{\mathrm{q}}}, \tag{3.11b}$$

(iii) Associated production of gluinos and scalar-quarks

$$\mathrm{qg} \to \tilde{\mathrm{q}}\tilde{\mathrm{g}}. \tag{3.12}$$

(iv) Associated production of gluinos and photinos

$$\mathrm{q\bar{q}} \to \tilde{\mathrm{g}}\tilde{\gamma}. \tag{3.13}$$

(v) Associated production of scalar-quarks and photinos

$$\mathrm{q\bar{g}} \to \tilde{\mathrm{q}}\tilde{\gamma}. \tag{3.14}$$

We have computed the squared matrix elements for all the processes listed above. They are discussed further in appendix A, where there are figures showing these processes.

Other production processes such as scalar-quark production from a gluino component inside the proton (which may be relevant if gluinos are light) and 2-to-3 processes such as $gg \to \tilde{g}\tilde{g}g$ will be discussed later on in this section.

Notice that we have only listed processes which involve scalar-quarks, gluinos and photinos. Clearly, there are other supersymmetric particles which can be produced at hadron colliders and can lead to missing-energy events. For example, pairs of neutralinos or charginos, the partners of gauge and Higgs bosons, can be produced at hadron-colliders (e.g., $q\bar{q} \to \tilde{\chi}^+\tilde{\chi}^-$, $q\bar{q} \to \tilde{\chi}^0\tilde{\chi}^0$) via the standard Drell-Yan mechanism or by scalar-quark exchange [32–34]. Typical decay processes such as $\tilde{\chi} \to q\bar{q}\tilde{g}$ (or $\tilde{\chi} \to q\bar{q}\tilde{\gamma}$ if the gluino is heavy) could lead to missing-energy signatures similar to the ones which can occur from scalar-quark and gluino production. In particular, $q\bar{q} \to \tilde{\chi}_1^0\tilde{\chi}_2^0$ can lead to distinctive one-sided events if $\tilde{\chi}^0$ is the lightest supersymmetric particle [33]. Nevertheless, we will omit these possibilities from the analysis presented in this paper for two basic reasons. First, because scalar quarks and gluinos are strongly interacting particles, their production rates are significantly larger than those of charginos and neutralinos of the same mass. Of course, if a significant number of missing-energy events are seen above background, this does not necessarily imply that the scalar-quark and/or gluino is the best possible supersymmetric explanation.

Second, the analysis for scalar-quarks and gluinos requires the fewest number of model assumptions as discussed in sect. 2. In the case of charginos and neutralinos, unknown mixing angles and many possible decay patterns makes it very difficult to set hard limits on possible supersymmetric masses. This is already evident from observing the complicated limits on chargino and neutralino masses obtained by the PETRA and PEP experimental groups [35]. (One can of course make specific tests of particular models which fix the various unknown supersymmetric parameters. See, e.g., ref. [34].)

We now turn to the decay process. Here, we must consider two separate cases which lead to quite different types of signatures.

Case 1: $M_{\tilde{g}} > M_{\tilde{q}}$. In this case the gluino decays (nearly) 100% of the time via:

$$\tilde{g} \to q\bar{\tilde{q}} \quad \text{or} \quad \tilde{q}\bar{q}, \tag{3.15}$$

where the sum is taken over all possible quark flavors which are kinematically accessible. The scalar-quark decays (nearly) 100% of the time via:

$$\tilde{q} \to q\tilde{\gamma}. \tag{3.16}$$

We shall neglect other rarer decay modes, although one should keep in mind that if

there exists a light chargino or neutralino other than the photino such that $M_{\tilde{\chi}} < M_{\tilde{q}}$, then the decay $\tilde{q} \to q\tilde{\chi}$ could be significant.

Case 2: $M_{\tilde{g}} < M_{\tilde{q}}$. In this case the gluino decays via processes (3.15) and (3.16) where the scalar-quark is virtual:

$$\tilde{g} \to q\bar{q}\tilde{\gamma}. \tag{3.17}$$

Again, one must sum over all quark flavors which are kinematically accessible. A sum over $\tilde{q}_L$ and $\tilde{q}_R$ intermediate states is assumed. In the case of the scalar quark, two decay modes are allowed (making assumptions similar to those above) with branching ratios (B) as indicated:

$$\tilde{q} \to \begin{cases} q\tilde{g}, & B = \dfrac{r}{1+r} \\ q\tilde{\gamma}, & B = \dfrac{1}{1+r}, \end{cases} \tag{3.18}$$

where $r \equiv \alpha_s/(e_q^2\alpha)$. Note that the dominant scalar-quark decay is $\tilde{q} \to q\tilde{g}$; the gluino then decays via eq. (3.17). This is the main reason for the difference in signatures between cases 1 and 2. In case 1, scalar-quark decay leads to substantial missing energy via the process given by eq. (3.16). In case 2, the dominant process is $\tilde{q} \to q\tilde{g}, \tilde{g} \to q\bar{q}\tilde{\gamma}$ leading to far less missing energy as compared with case 1. Practically speaking, this means that if $M_{\tilde{q}} > M_{\tilde{g}}$, it will be very difficult to isolate $\tilde{q}\bar{q}$ production; in this case, $\tilde{g}\tilde{g}$ production will be the main process that should be looked for.

According to eq. (3.8), we need expressions for the matrix elements for the above decay processes. We also need explicit expressions for the scalar-quark and gluino widths. These are given in appendix A.

3.2. HIGHER ORDER PROCESSES

The production processes listed in eqs. (3.9)–(3.14) represent contributions to the lowest order approximation to the inclusive production cross-section of supersymmetric processes. Let us focus here on gluino pair production: $p\bar{p} \to \tilde{g}\tilde{g} + X$. To $\mathcal{O}(\alpha_s^2)$, the processes which contribute have been given in eq. (3.9). If we consider $\mathcal{O}(\alpha_s^3)$, we must include loop corrections to the processes given by eq. (3.9), and in addition we must introduce new $2 \to 3$ processes:

$$gg \to \tilde{g}\tilde{g}g, \tag{3.19}$$

$$q\bar{q} \to \tilde{g}\tilde{g}g, \tag{3.20}$$

$$gq \to \tilde{g}\tilde{g}q. \tag{3.21}$$

If the perturbative series is trustworthy, then we should find that the $\mathcal{O}(\alpha_s^3)$

contributions are smaller than the $\mathcal{O}(\alpha_s^2)$ Born terms. However, Herzog and Kunszt [36] realized that when various triggers and cuts are applied to the total cross section, it is possible that the $\mathcal{O}(\alpha_s^3)$ contributions are enhanced significantly. In fact, we find that this indeed occurs for certain ranges of values of the gluino mass when the UA1 triggers and cuts are imposed. To explain the effect, consider the consequences of requiring that the missing transverse energy be larger than some fixed number: $E_T^{\text{miss}} > E_0$. Suppose that the gluino is light (say, 5 GeV). Then in general, $\tilde{g}\tilde{g}$ events will not survive the E_T^{miss} cut. The reason is that light gluinos are typically quite energetic. Since to a very good approximation, the transverse momenta of the gluinos are entirely generated by the hard subprocess, their transverse momenta are nearly back-to-back. When the gluinos decay ($\tilde{g} \to q\bar{q}\tilde{\gamma}$), the two photinos will be nearly back-to-back. Since $E_T^{\text{miss}} = |\boldsymbol{p}_{T1}^{\tilde{\gamma}} + \boldsymbol{p}_{T2}^{\tilde{\gamma}}|$, we see that E_T^{miss} will in general be small and these events will fail to pass the E_T^{miss} cut. How then do any $\tilde{g}\tilde{g}$ events survive the cut? If the decays of the two gluinos are sufficiently asymmetric, it is possible to generate $E_T^{\text{miss}} \geq E_0$. As $M_{\tilde{g}}$ becomes *smaller*, $\sigma_{\text{total}}(p\bar{p} \to \tilde{g}\tilde{g} + X)$ increases rapidly, while at the same time, the probability that a $\tilde{g}\tilde{g}$ event passes the cut decreases rapidly. When fragmentation effects are taken into account, one finds that $\sigma(p\bar{p} \to \tilde{g}\tilde{g} + X)$ subject to the E_T^{miss} cut actually decreases as $M_{\tilde{g}}$ becomes smaller for $M_{\tilde{g}} \lesssim 20$ GeV.

Now, consider the effect of the E_T^{miss} cut on the processes given by eqs. (3.19)–(3.21). If the final state gluon (or quark) is hard, then a possible configuration is one where the $\tilde{g}\tilde{g}$ pair is emitted in the same hemisphere recoiling against the gluon (or quark). In this configuration, the photinos resulting from the gluino decays are often emitted in the same hemisphere so that it is much easier to have $E_T^{\text{miss}} = |\boldsymbol{p}_{T1}^{\tilde{\gamma}} + \boldsymbol{p}_{T2}^{\tilde{\gamma}}| \geq E_0$. Of course, the cross section for the $2 \to 3$ processes decreases as the transverse momentum of the hard gluon (or quark) increases. Nevertheless, it is clear that the $2 \to 3$ processes of eqs. (3.19)–(3.21) are more likely to survive the E_T^{miss} cut than the $2 \to 2$ processes. So, it is conceivable that when the E_T^{miss} cut is applied, the $2 \to 3$ processes will result in *more* events passing the cuts as compared with the $2 \to 2$ processes. This indeed occurs as first shown by Herzog and Kunszt. As discussed in sect. 7, we confirm their results and show that this has very important consequences for whether light gluinos are excluded by the data.

At present, a full $\mathcal{O}(\alpha_s^3)$ calculation does not exist. The Born terms for the $2 \to 3$ processes (eqs. (3.19)–(3.21)) have been obtained by Herzog and Kunszt [36]. In order to use their results, one must impose a cut-off on the transverse momentum of the outgoing gluon (or quark). Otherwise, one would be plagued with infrared and collinear singularities which would be cancelled by the $\mathcal{O}(\alpha_s^3)$ loop corrections. (Note that the only collinear singularities which occur here are those that arise when the outgoing gluon or quark is parallel to an *initial* parton. No collinear singularities result when the outgoing gluon or quark is parallel to an outgoing gluino due to the non-zero gluino mass. Hence, a p_T cut-off on the outgoing gluon or quark is sufficient to protect against both infrared and collinear infinities.) The question then

arises: How should this p_T cut-off be chosen? If the p_T cutoff is too small, then one is liable to overestimate the effect of the $2 \to 3$ process since the effect of virtual $\mathcal{O}(\alpha_s^3)$ processes (which are not included in the analysis) can be negative thereby reducing the final result. It may appear unlikely that the virtual graphs which are $2 \to 2$ processes and therefore occur at $p_T = 0$ (where $\boldsymbol{p}_T = \boldsymbol{p}_{T1}^{\tilde{g}} + \boldsymbol{p}_{T2}^{\tilde{g}}$) could affect results at $p_T \neq 0$. However, we are not dealing with infinitely narrow jets (a Sterman-Weinberg [37] type analysis is appropriate here). When the finite resolution of partonic jets is taken into account, one indeed finds that negative virtual $2 \to 2$ graphs can affect the results if the p_T cutoff is too small. On the other hand, if the p_T cutoff is too large, then the resulting $2 \to 3$ cross-section is too small and one is missing a potentially important affect. As advocated by Herzog and Kunszt, we take $p_T^{\text{cutoff}} = 10$ GeV. Basically, the choice $p_T^{\text{cutoff}} \gtrsim M_{\tilde{g}}$ should certainly be safe from the effects of the virtual graphs, and if anything, such a choice is conservative and would underestimate the effect of the $2 \to 3$ processes. Details of the numerical effect of the $2 \to 3$ processes are discussed in sect. 7.

If and when the full $\mathcal{O}(\alpha_s^3)$ correction is calculated, one has ways of "improving" the lowest order prediction by choosing a particular scale in the running coupling constant which minimizes the $\mathcal{O}(\alpha_s^3)$ correction. When an appropriate choice is made, it is often found that the first non-trivial QCD corrections are small (say, less than about 20% at Sp$\bar{\text{p}}$S energies). Given that the full $\mathcal{O}(\alpha_s^3)$ corrections have not been computed here, we must simply accept the fact that the computations laid out in subsect. 3.1 have an uncertainty. We will summarize the theoretical uncertainties of the perturbative QCD framework in subsect. 3.4.

3.3. THE DISTRIBUTION OF GLUINOS INSIDE A PROTON

The best available limits on gluino masses (excluding the Sp$\bar{\text{p}}$S collider data) are obtained from beam dump experiments [38–39] and are somewhere in the vicinity of 3 GeV (the precise limit depends on the scalar-quark mass). Suppose that the gluino mass is on the order of 5 GeV, i.e., slightly heavier than the minimum mass allowed by the beam dump experiments. Henceforth, we shall refer to this case as the light gluino scenario. Such a gluino has properties very similar to that of a b-quark with one important exception: the gluino is a color octet fermion compared with the color triplet b-quark. This seemingly small detail has large consequences. The production cross section of such a gluino would be an order of magnitude larger than that of the b-quark. This fact is due to the larger color factors associated with the hard scattering processes which produce the gluino (here, the dominant production mechanism is gluon-gluon scattering).

For light gluinos, the possibility arises that they may make up a non-negligible fraction of the momentum of the proton. This can occur via the perturbative process where a gluon (which is observed as a constituent of the proton at a scale Q_0^2) splits into a $\tilde{g}\tilde{g}$ pair. Thus, at a scale Q^2, one would predict the presence of gluino

constituents inside the proton. Perturbative QCD allows one to predict the evolution of the distribution function $f_{\tilde{g}}(x, Q^2)$ for the gluino component of the proton [40]. To leading order in α_s and ignoring corrections of order $M_{\tilde{g}}^2/Q^2$,

$$f_{\tilde{g}}(x, Q^2) = \frac{\alpha_s(Q^2)}{2\pi} \sum_j \int_x^1 \frac{dy}{y} P_{\tilde{g}j} f_j(y, Q^2), \tag{3.22}$$

where $P_{\tilde{g}j}$ are the Altarelli-Parisi splitting functions [41] which describe the probability that parton j splits into two other partons, one of which is the gluino which is "seen" as a constituent of the proton. Eq. (3.22) represents a set of coupled integro-differential equations. To a first approximation, we may take $f_j(y, Q^2)$, for j = quark or gluon, to be the standard quark or gluon distribution functions as obtained by any of the standard analyses. Furthermore, a boundary condition is required for $f_{\tilde{g}}(x, Q^2)$. We choose $f_{\tilde{g}}(x, Q_0^2) = 0$ for $Q_0^2 = 4M_{\tilde{g}}^2$, and use the threshold behavior described in ref. [9]. Scalar quarks are ignored in this analysis, as they are assumed to be heavy in the light gluino scenario. In a more exact treatment, one would have to recompute the quark and gluon distribution functions as a result of having included a non-zero gluino component. The effects of such a correction are undoubtedly small in the present context (i.e., for predictions at the Sp$\bar{p}$S Collider).

We show in fig. 1 an example of the resulting gluino distribution in the case of $M_{\tilde{g}} = 5$ GeV and $Q^2 = (100\ \text{GeV})^2$. For comparison, the gluon distribution function is also shown at the same value of Q^2. Note that the gluino distribution function is indeed small (less than 1% of the gluon distribution) yet not vanishingly small. One reason for this is again connected with the color octet nature of the gluino.

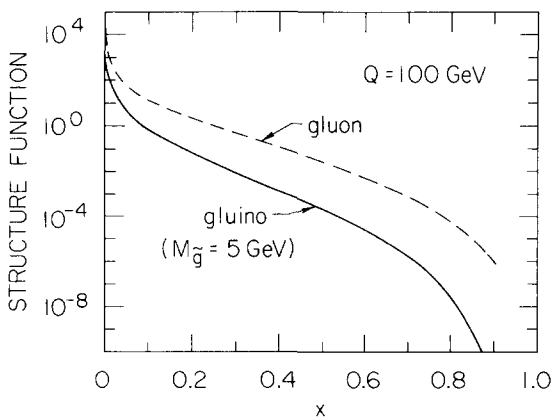

Fig. 1. The structure function of the gluino versus x when $M_{\tilde{g}} = 5$ GeV and $Q = 100$ GeV. The gluon structure function is shown with a dashed curve for comparison.

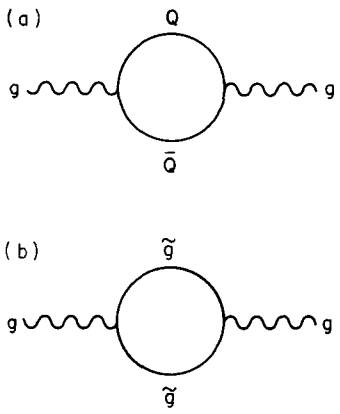

Fig. 2. Feynman graphs for calculating the Altarelli-Parisi splitting functions for (a) $g \to Q\bar{Q}$ (Q = heavy quark) and (b) $g \to \tilde{g}\tilde{g}$.

Comparing the color factors that arise from fig. 2a and b,

$$\text{fig. 2a:} \qquad \mathrm{Tr}T^a T^b = \tfrac{1}{2}\delta^{ab}, \tag{3.23a}$$

$$\text{fig. 2b:} \qquad f_{acd}f_{bcd} = 3\delta_{ab}, \tag{3.23b}$$

it follows that $P_{\tilde{g}g}(y) = 6P_{Qg}(y)$, where Q is a heavy quark, which implies that:

$$f_{\tilde{g}}(x, Q^2) \approx 6f_b(x, Q^2) \tag{3.24}$$

assuming that $M_{\tilde{g}} = m_b$.

The perturbatively generated gluinos in the proton may be very important [20] in determining the missing energy events expected in the light gluino case. The reason is that new hard scattering processes must now be considered:

$$\tilde{g} + q \to \tilde{q} \tag{3.25}$$

followed by the subsequent decay of the final state supersymmetric particle. In addition, there are new $2 \to 2$ scattering processes:

$$\tilde{g} + q \to \tilde{q} + g, \tag{3.26}$$

$$\tilde{g} + q \to \tilde{g} + q, \tag{3.27}$$

$$\tilde{g} + g \to \tilde{g} + g, \tag{3.28}$$

$$\tilde{g} + g \to \tilde{q} + \bar{q}. \tag{3.29}$$

The most important process to consider in the context of the missing energy events is

eq. (3.25). The new $2 \to 2$ scattering processes given by eqs. (3.26)–(3.29) are numerically less significant than the $2 \to 1$ process given by eq. (3.25).

Eq. (3.25) can be very efficient for the production of events with large E_T^{miss}. For example, if $\tilde{q} \to q + \tilde{\gamma}$, then $E_T^{miss} \approx \frac{1}{2} M_{\tilde{q}}$. This is just a consequence of the jacobian peak analogous to that which is seen in the missing energy spectrum which results from W decay. Of course, this decay mode is disfavored as shown in eq. (3.18) since the scalar-quark is assumed to be heavier than the gluino. The dominant decay is $\tilde{q} \to q\tilde{g} \to qq\bar{q}\tilde{\gamma}$; including fragmentation effects, the resulting E_T^{miss} spectrum due to the photino is softened to such an extent, it turns out that the rarer $\tilde{q} \to q + \tilde{\gamma}$ decay dominates the missing energy events for the light gluino scenario if fragmentation and UA1 cuts and triggers are applied.

An important issue regarding the gluino distribution function has been raised by Barger et al. [18] in a recent paper. First, they remark that since gluinos in the proton have resulted from $g \to \tilde{g}\tilde{g}$, the process given by eq. (3.25) is in reality:

$$g + q \to \tilde{g} + \tilde{q}, \tag{3.30}$$

where the final state gluino goes near the forward direction due to the kinematics of the process in which the gluino is light and the scalar-quark is heavy. They note that if the gluino distribution function as derived in eq. (3.22) is used, then surprisingly, eq. (3.25) results in a larger cross section than does eq. (3.30); the relative factor for $M_{\tilde{g}} = 5$ GeV is a factor of 2 to 4 depending on what value of Q_0 is chosen as a boundary condition to set $f_{\tilde{g}}(x, Q_0^2) = 0$. They next comment that eq. (3.22) represents a leading-log computation which can be "reproduced" by computing process (3.30) in the approximation that terms in $\sigma(g + q \to \tilde{g} + \tilde{q})$ not proportional to $\log(M_{\tilde{g}}^2/M_{\tilde{q}}^2)$ are dropped. Finally, they argue that the terms that were dropped in the latter computation are important at the energies and masses of interest. In fact, these terms are negative, which explains why the predictions of eq. (3.25) were so much larger than that of eq. (3.30). Their conclusion is that to a good approximation, one should simply neglect the gluino component of the proton at $Sp\bar{p}S$ energies and simply use eq. (3.30) along with all the other $2 \to 2$ processes discussed in subsect. 3.1.

For the most part, we agree with the analysis of Barger et al. [18]. However, it is important to keep in mind that the solution of the Altarelli-Parisi [41] equations (eq. (3.22)) sums up, to leading log, the emission of multiple gluons. Thus, the use of the gluino structure function incorporates processes beyond that of the simple $2 \to 2$ process given by eq. (3.30). However, this leading log approach can only be justified if

$$\alpha_s(Q^2) \log \frac{Q^2}{M_{\tilde{g}}^2} \gg 1. \tag{3.31}$$

Here, the relevant $Q^2 \equiv M_{\tilde{q}}^2$. For $M_{\tilde{q}} = 100$ GeV and $M_{\tilde{g}} = 5$, eq. (3.31) is not

satisfied; in fact $\alpha_s \log(M_{\tilde{q}}^2/M_{\tilde{g}}^2) \sim 1$. This suggests that non-leading log effects can be important, and indeed this is what Barger et al. found. If eq. (3.31) were justified, then one could properly omit process (3.30) from consideration, and instead compute the gluino structure function and consider processes (3.25)–(3.29). However, in the present case, we believe that neglecting the gluino content of the proton and including process (3.30) would probably result in only a very slight underestimate of the missing energy signal.

Ironically, the UA1 collaboration has introduced a new trigger in their 1984 [23, 42] run which significantly enhances the $\tilde{g}\tilde{g}$ production processes (eq. (3.9)) with respect to both eqs. (3.25) and (3.30) (see sects. 5 and 7 for further details). As a result, the uncertainty of the relevance of the gluino structure function has in fact become a moot point regarding the analysis of the 1984 data. Nevertheless, the issues discussed above are of interest from a theoretical point of view and have relevance to heavy quark production in general.

3.4. UNCERTAINTIES DUE TO PERTURBATIVE QCD

Here, we summarize what we think are the uncertainties in the calculations presented in this section. First, in the calculation involving the $2 \to 2$ hard scattering subprocess, one has to choose a set of parton distribution functions and a value for Λ. We have chosen $\Lambda = 0.29$ GeV and use the EHLQ structure functions [9] corresponding to this choice. We choose the running coupling constant with dependences on the b- and t-quark thresholds as given in ref. [9]. However, we neglect the effect of supersymmetric particle masses on the running of the coupling constant. We choose to evaluate the running coupling constant $\alpha_s(Q^2)$ in eq. (3.1) at $Q^2 = \hat{s}$. One might also choose other possible values (e.g., $Q^2 = p_T^2$), although, without a full computation of the $\mathcal{O}(\alpha_s^3)$ correction, such a choice is somewhat arbitrary. The higher order corrections are neglected ("no K-factor is used," to use the unfortunate but prevalent jargon), except that we do investigate the effects of a hard $2 \to 3$ partonic subprocess (in particular, eq. (3.19)) where by "hard," we mean that the transverse momentum of the radiated gluon satisfies $p_T > 10$ GeV. We have computed the distribution of light gluinos inside the proton and have compared processes given by eqs. (3.25) and (3.30). Each step discussed above has some uncertainty. Overall, we feel that the calculation up to this point is certainly reliable to within a factor of two. We would be hard pressed to claim the ability to make a more accurate prediction at this time, especially given that one observes hadronic jets in the final state rather than the original final-state partons.

4. The Monte Carlo event generator

In sect. 3, we outlined the relevant formulas for computing the cross section for $p\bar{p} \to$ final state partons. Of course, the calorimeters of the UA1 and UA2 detectors

measure energy deposition of final state hadrons and *not* the partons themselves. Furthermore, a given event contains far more activity than a hard $2 \to 2$ (or even $2 \to 3$) scattering. One can make a list of many effects which clearly take place which are not included in the simple parton formalism. Such a list would include: initial-state gluon radiation, final-state gluon radiation, fragmentation and hadronization of final state partons, interaction of spectators; recombination of spectators into color singlet final states, etc. In comparing a theoretical prediction with actual experimental results, all these effects must be accounted for in some way. In constructing our Monte Carlo event generator, we have decided to incorporate these effects only in the crudest way. To do anything more sophisticated would be pointless – without making use of a full detector simulation appropriate for analyzing the results of a given experiment. This is clearly the job of the experimental groups themselves. We shall argue however that even with our crude implementation of "real world" effects beyond the parton model, we will be in a position to obtain reasonable estimates of the magnitude of various differential cross sections of interest as well as the effects of triggers and cuts imposed by the various experiments. This will enable us to estimate which ranges of supersymmetric particle masses are allowed or ruled out given the current data. Precise limits must await a more complete analysis by the experimental groups at the CERN $S\bar{p}pS$.

The procedure of our Monte Carlo event generator is as follows. We perform the integration given by eq. (3.1) by Monte Carlo techniques; the result is a series of four-momenta for all final state particles (which result after the decay of all intermediate states). Each set of four-momenta is called an "event." For example, if the hard scattering was $gg \to \tilde{g}\tilde{g}$ followed by $\tilde{g} \to q\bar{q}\tilde{\gamma}$, an event would consist of six four-momenta of two quarks, two antiquarks and two photinos respectively. The parton four-momenta obtain in this way are interpreted as jets as observed in the calorimeters of real experiments. This is a major approximation – hadronization of final state quarks and gluons is omitted. (Such a method has been recently dubbed the "parton Monte Carlo.") Such an approximation will preclude us from studying many aspects of the data. For example, we cannot calculate jet multiplicities and single jet masses. Nevertheless, such a procedure probably does not do so badly in estimating the gross features of the data: e.g., p_T distribution of jets, two-jet invariant masses, etc. One indication of the validity of this approach is evidenced by the results of Ellis and Kowalski [16] who have compared the results of a parton-Monte Carlo and a Monte Carlo including hadronization. They found that the differences were small for the quantities we consider.

In our previous paper [19] and other early papers on this subject, fragmentation effects were ignored; however, these effects can play an important role in determining the missing E_T spectrum of a given event. For example, a gluino which is produced by some hard process must first "fragment" into a supersymmetric hadron (say a $g\tilde{g}$ or $\tilde{g}q\bar{q}$ bound state) which then decays weakly, emitting a photino which escapes the detector. If the momentum of the gluino inside the supersymmetric

hadron is less than that of the original gluino, then the photino spectrum will be degraded compared to the spectrum which would have resulted had fragmentation been ignored. Let us define z to be the momentum fraction of the gluino (or scalar-quark) inside the supersymmetric hadron. For large gluino or scalar-quark masses the z-distribution is sharply peaked at $z = 1$, and fragmentation effects are not relevant in determining the missing energy spectrum (due to the outgoing photinos). However, for gluino or scalar-quark masses less than about 20 GeV, fragmentation becomes increasingly important and the result is a missing energy spectrum which is softer than it would have been had fragmentation been ignored.

The implementation of fragmentation effects is a delicate procedure. One must be sure to conserve energy-momentum in the process, and different procedures have been shown to yield quite different results in the detailed structure of the events. We account for these uncertainties in determining the reliability of our final results. Our procedure consisted of three steps, which we shall illustrate using $gg \to \tilde{g}\tilde{g}$ as an example. Step one was to generate the initial hard scattering $gg \to \tilde{g}\tilde{g}$, the result of which is two four-momenta of the two outgoing gluinos. Step two was to generate a momentum fraction z by which we degrade the momenta of each final state gluino. Such a z is generated at random according to a distribution suggested by De Rújula and Petronzio [21]. We take the distribution to be:

$$D(z, \hat{s}) = \int_0^1 \mathrm{d}x\, \mathrm{d}y\, \delta(z - xy) D_1(x, \hat{s}) D_2(y), \tag{4.1}$$

$$D_1(x, \hat{s}) = A(1 - x)^{A-1}, \tag{4.2}$$

$$A = \tfrac{36}{25} \log\left[\log(\hat{s}/\Lambda^2)/\log(4M_{\tilde{g}}^2/\Lambda^2)\right], \tag{4.3}$$

$$D_2(x) = \frac{Nx(1-x)^2}{\left[(1-x)^2 + \varepsilon x\right]^2}, \tag{4.4}$$

$$\varepsilon = \left(\frac{0.6\ \mathrm{GeV}}{M_{\tilde{g}}}\right)^2, \tag{4.5}$$

where $\Lambda = 0.29$ GeV and N is normalized such that

$$\int_0^1 D_2(x)\, \mathrm{d}x = 1. \tag{4.6}$$

$D_2(x)$ represents the non-perturbative contribution to fragmentation as advocated by Peterson et al. [43] and $D_1(x, \hat{s})$ is an approximation to the perturbative fragmentation due to gluon emission of the produced gluino. One could be more

sophisticated and replace $D_1(x, \hat{s})$ above by a fragmentation function generated by solving the appropriate Altarelli-Parisi equations as was done by Barger et al. [18]. The results of these two procedures are similar, so we have opted for the simpler one to minimize computer time. Note that $D(z, \hat{s})$ depends on $\hat{s}$, the partonic center-of-mass energy squared.

Given a gluino of four momentum $(E; \boldsymbol{p})$, we replace it with a new four-momentum $(E'; \boldsymbol{p})$, where E' is chosen such that $M_{\tilde{g}}^2 = [E'^2 - z^2\boldsymbol{p}^2]^{1/2}$. We then impose energy-momentum conservation by forming the remaining four-vector $(E - E', (1 - z)\boldsymbol{p})$. This four-vector is necessarily space-like since an on-shell massive particle cannot decay into an on-shell massive particle of the same mass plus a physical particle (with a time-like four-momentum). We shall proceed, nevertheless, temporarily ignoring this problem. The important effect of fragmentation, namely the degraded missing energy spectrum, is obtained by decaying the $\tilde{g}$ with four-momentum $(E'; \boldsymbol{p})$ into $q\bar{q}\tilde{\gamma}$. Finally, the left-over space-like vector is added back (arbitrarily) into the $q\bar{q}$ final state system. Although this procedure seems ad hoc, we emphasize that fragmentation effects are only important for very light gluinos. In this case, the gluinos produced at the Sp$\bar{p}$S will be quite energetic so that the decay products plus the fragments will be moving roughly in the same direction in the laboratory and will be interpreted as one jet by the jet-finding algorithm (see sect. 5 for a description of this algorithm).

At this point, an event consists of final state jets, missing transverse energy and clusters which were not energetic enough to be defined as jets by the UA1 jet criterion. However, this final state has resulted entirely from the Born approximation to the hard constituent scattering. We have, so far, neglected a number of important effects: the possibility of gluon radiation, the effects of the remnants of the original p and $\bar{p}$ which are colliding, the generation of hadrons in the color neutralization of the final state jets, etc. Consider the effects on the final state jets themselves. First, a jet can lose energy – in the fragmentation process or in gluon bremstrahlung. Second, the jet can gain energy – particles not involved in the hard scattering can stray into the cone which defines the jet in question. All in all, one can imagine that the prediction of jet distributions (e.g., the E_T^{jet} distribution) will be only marginally changed by including such effects. Only the single jet multiplicities and invariant masses are totally unreliable (where hadronization plays a crucial role).

An important quantity to consider is the total scalar transverse energy of an event denoted by E_T. This is defined experimentally by adding in a scalar fashion the transverse energy deposited in all calorimeter cells. This quantity is used by the UA1 collaboration in defining one of the triggers (see sect. 5) and one of the missing energy cuts so we must consider it here in detail. It is clear that such a quantity is incalculable in the framework of perturbative QCD; in particular, the sum of the scalar transverse energies of the final-state jets is a severe underestimate of the value of E_T. To get an idea of the magnitude of such an underestimation, consider p$\bar{p}$

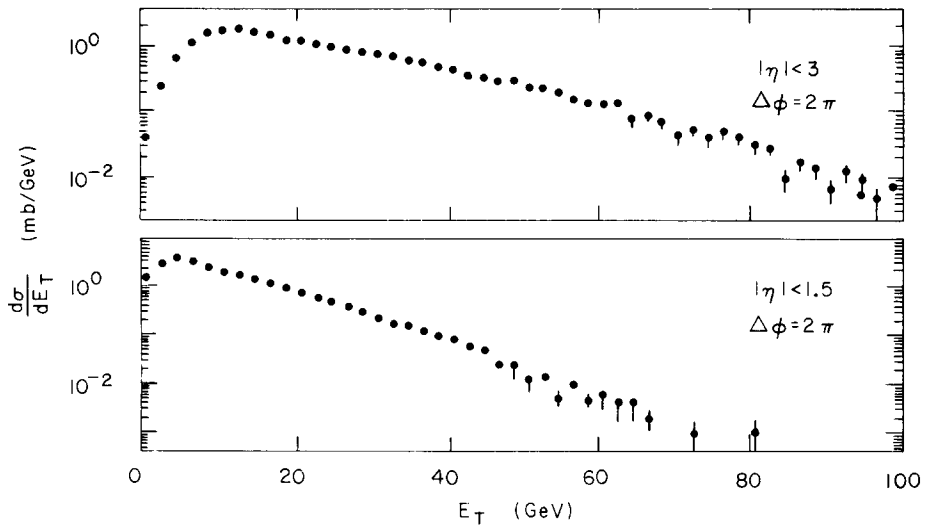

Fig. 3. The E_T distribution observed by the UA1 collaboration for events with no large p_T jets ("minimum-bias" events), taken from ref. [44]. The distribution shown in the upper plot ($|\eta| < 3$) used for the "remainder" portion of hard-scattering events was based on this distribution, but scaled so the average E_T was much larger (see text). The distribution shown in the lower plot ($|\eta| < 1.5$) is similarly rescaled and used in conjunction with the third trigger (eq. (5.24)).

collisions with *no* large p_T jets in the final state (the so-called "minimum bias" events). The UA1 collaboration has obtained the E_T distribution of such events [44], which we reproduce here in fig. 3. A noteworthy feature of the upper distribution is the long non-gaussian tail at both low and high E_T. Quantitatively, the mean of this distribution (24 GeV) is quite different from the median (18 GeV) and both numbers are larger than the value of E_T where the distribution peaks (12 GeV). To obtain E_T in our parton-Monte Carlo, one is tempted to superimpose a minimum-bias event on top of the underlying hard scattering. In fact, this is known to be incorrect. If one studies the UA1 and UA2 samples [45–46] of large-p_T two jet events, and subtracts out the two jets in each event, the E_T distribution of the "remainder" is substantially harder, roughly twice that of minimum bias. We will use the term "remainder" below with this technical meaning.

UA2 has further reported [46] that for $\Sigma p_T^{jet} > 15$–20 GeV (which is always true for the missing energy events considered), the energy of the remainder is roughly independent of Σp_T^{jet}. Qualitatively, such an effect is due in part to initial-state radiation which occurs when the constituents which participate in the hard scattering are pulled out the p and $\bar{p}$ and in part to the final-state radiation of the final state quarks and gluons in the process of fragmentation and hadronization. In order to proceed with the analysis of supersymmetric particle production, one needs to know the E_T distribution of the remainder in order to compute the E_T of a given Monte

Carlo event. On the basis of the discussion above, it is likely that the remainder E_T distribution in events with supersymmetric particle production will be roughly twice that of minimum bias (in analogy to the two jet events). However, it is at present unknown how to theoretically compute the remainder E_T distributions given a hypothetical hard scattering subprocess. Furthermore, the hadronizing Monte Carlo programs in existence today were for the most part developed for $e^+e^- \to$ hadrons where the problems of initial-state radiation do not arise. Monte Carlo routines which reproduce the correct remainder distributions appropriate for hadron colliders have not been fully developed [47]. Given this current state of ignorance, we have decided on the following course of action. We have rescaled the upper E_T distribution shown in fig. 3 by a factor of 1.67 such that the mean is 40 GeV. (In fact, the median of our rescaled distribution is 32 GeV.) We have found the following parameterization to be convenient:

$$\frac{CE_T^2}{E_T^2 \exp(bE_T) + a}, \tag{4.7}$$

where $a \approx 257$ and $b \approx 0.036$. For each event obtained by our parton-Monte Carlo, we choose an additional random value for the remainder transverse energy (denoted by E_r) based on the distribution given by eq. (4.7). The total scalar transverse energy is then given by

$$E_T = \sum_{\text{jets}} E_{Ti} + \sum_{\substack{\text{low} \\ \text{energy} \\ \text{clusters}}} E_{Ti} + E_r, \tag{4.8}$$

where by "low energy clusters," we mean clusters which were not called jets since their transverse energy was below the jet threshold.

Let us denote:

$$E_T^{\text{extra}} = E_T - \sum_{\text{jets}} E_{Ti}. \tag{4.9}$$

From our discussions above, we expect the distribution of E_T^{extra} to be roughly twice that of minimum bias (i.e., with a mean of about 50 GeV). We have found in our computations that

$$\sum_{\substack{\text{low} \\ \text{energy} \\ \text{clusters}}} E_{Ti} \approx 10 \text{ GeV} \tag{4.10}$$

in the mean. (This value is closely tied to the assumed value for the jet threshold.) This explains why we chose E_r based on a distribution whose mean was 40 GeV. In studying the monojet events, we can study the published data and compute $E_T^{\text{extra}} = E_T - E_T^{\text{monojet}}$ on an event-by-event basis. Although the statistics are quite low, we

find that E_T^{extra} is distributed with a mean of about 50 GeV, in agreement with the discussion above.

The precise choice for E_r can have a tremendous impact on the number of events which pass the UA1 missing energy trigger. This is unfortunate given that E_r is not so well understood theoretically. This uncertainty will be an important factor in determining the reliability of our final numbers. This will be discussed in sect. 6.

To summarize, we have constructed a Monte Carlo event generator in which final-state partons produced by a hard scattering process are interpreted as energy clusters. Missing transverse energy results from photinos which are emitted by decaying gluinos or scalar-quarks which are produced in the hard scattering event. Fragmentation of gluinos (or scalar-quarks) can be important if the mass of the gluino is less than 20 GeV. The main effect of fragmentation is to reduce the momentum of the decaying gluino thereby reducing the missing energy resulting from the escaping photino. The observable energy clusters remaining in the final state are passed through a jet algorithm and interpreted as jets if their energy is above the jet threshold. Finally, a remainder transverse energy, E_r, is generated on an event-by-event basis in order to calculate the total scalar transverse energy, E_T, of a given event.

5. Modeling experimental conditions

Although the details of our simulation of UA1 experimental conditions [23] may not make exciting reading, they are critical to the validity of our results (especially for the question of a light gluino). Furthermore, an understanding of these experimental conditions, which include triggers, cuts, resolution and efficiencies, is essential if one is to attempt an extrapolation to the Tevatron Collider or the Superconducting Super Collider (SSC).

On the basis of extensive consultations with members of the UA1 Collaboration, we have arrived at a procedure for simulating the UA1 conditions. Our approach is not at all the same as those used by others who have analyzed the UA1 data. It is important to understand that no Monte Carlo calculation can precisely duplicate real events which come from experiment. At times, one must introduce a Monte Carlo procedure which is somewhat different from the actual experimental analysis. Nevertheless, we feel that the procedures we have employed succeed in providing a good approximation to the UA1 methods. We have run tests to determine the magnitude of uncertainties introduced into our results by varying our procedures. These are described in sect. 6.

Our description of experimental conditions follows not the logic of the experiment, but rather the logic of a theorist's Monte Carlo which generates the 4-momenta of all final-state partons. This Monte Carlo then modifies the momenta to simulate detector and fragmentation effects and tests them against trigger and cut requirements.

Before generating the final-state partons, there are two preliminaries. One may wish to give the initial-state partons a p_T distribution. This distribution is not, in general, well-known, and our tests have shown that there is little sensitivity to whether or not any such distribution is included. The results shown here have initial-state partons with zero p_T. Secondly, before generating each gluino decay, fragmentation effects "slow down" the gluino (as described in sect. 4). The "lost" momentum is then added onto the hadronic decay products of the gluino. The manner in which this is done is somewhat arbitrary; however, fragmentation effects are only important for light (fast-moving) gluinos where the resulting jets coalesce. Therefore it is not important how the momentum is added back in, nor is it likely that much energy will escape the jet cone.

There are sources of "fake" missing transverse energy. Recall that a given event consists of the jets (as determined by the jet algorithm) and the remainder, which has a mean transverse energy which is roughly twice that of minimum bias. One source of "fake" E_T^{miss} is due to the non-zero calorimetry resolution for the E_T of the remainder. While an experimentalist cannot distinguish unequivocally between the jets and the remainder portions of an event, a theorist's Monte Carlo obtains them independently. The generation of the E_T distribution of the remainder was discussed in sect. 4. Here we note that the resolution in transverse momenta is described by the distribution:

$$e^{-(\delta p_x)^2/2\sigma_x^2} e^{-(\delta p_y)^2/2\sigma_y^2}, \tag{5.1}$$

where for UA1

$$\sigma_x = \sigma_y = 0.5\sqrt{E_T^{extra}}, \tag{5.2}$$

$$E_T^{extra} \equiv E_T^{total} - \sum E_T^{jets}. \tag{5.3}$$

E_T^{extra} is the transverse energy of the remainder plus that of any clusters not passing the UA1 jet criterion. (We have oriented the co-ordinate system so that the beams define the z-axis.) Note that the UA1 Collaboration chooses to define a quantity:

$$\sigma' = \sqrt{\sigma_x^2 + \sigma_y^2} = \sqrt{2}\,\sigma_x = 0.7\sqrt{E_T^{extra}}. \tag{5.4}$$

For their E_T^{miss} cut, UA1 approximately combines this effect and that from jet resolution (see below) by use of

$$\sigma = 0.7\sqrt{E_T^{total}}. \tag{5.5}$$

The UA1 detector is somewhat inefficient in measuring jet momenta. While the precise value of this inefficiency is not known, they estimate [48] it at about 90%. We therefore reduce the momenta of jets by 10% to account for this effect.

The jet momenta are also subject to resolution effects (smearing), described in this case by

$$e^{-(\delta p_J)^2/2\sigma_J^2} \tag{5.6}$$

with

$$\sigma_J = 0.2 p_J , \tag{5.7}$$

where we make the approximation that $m(\text{jet}) \approx 0$. Note that this resolution (5.7) is not the same as that (5.2) for the remainder portion of the event.

As a result of the above smearing, each jet's momenta have changed so that "fake" missing transverse energy is generated. The resulting missing transverse momenta are:

$$\boldsymbol{p}_T^{\text{miss}} = \boldsymbol{p}_T \text{ (initial partons)} - \sum_i \boldsymbol{p}_{Ti} \text{ (outgoing smeared partons)} - \boldsymbol{p}_T \text{ (remainder)} . \tag{5.8}$$

Then

$$E_T^{\text{miss}} = \sqrt{p_{Tx}^{\text{miss2}} + p_{Ty}^{\text{miss2}}} . \tag{5.9}$$

Having smeared the momenta of the partons, it is now necessary to consider when the resultant jets would be coalesced into a single jet. Since we do not hadronize our partons, we cannot exactly follow the UA1 jet selection algorithm. But we imitated it at the partonic level. We begin by ordering our jet-partons by their E_T(jet(1) has the highest E_T, etc.).

If jet(1) and jet(2) satisfy the condition

$$(\Delta\phi)^2 + (\Delta\eta)^2 > 1 , \tag{5.10}$$

where ϕ is the azimuthal angle and η the pseudorapidity, then they are *not* coalesced (i.e., no action is taken). Next jet(1) and jet(3) are tested against condition (5.10) and if they again satisfy it, then no action is taken. We proceed in this manner until jet(1) has been tested against jet(n), $n = 2, 3, \ldots, N$. Assuming that condition (5.10) is satisfied at each step, we next test jet(2) against jet(n), $n = 3, 4, \ldots, N$ ending up finally with testing jet($N-1$) and jet(N).

If, however, at any stage, jet(i) and jet(j) ($i < j$) do not satisfy (5.10), then they are coalesced, and the resulting jet-parton is labelled as jet(i), and one proceeds on in the same manner except that there no longer is a jet(j).

Now one must decide whether a jet (parton) is to be called a jet or simply considered as additional transverse energy. The UA1 criterion is that

$$E_T^{\text{jet}} \geqslant 12 \text{ GeV} , \tag{5.11}$$

or it is not a jet. However, note that p_T^{jet} is the momentum after the 10% reduction and after smearing. If one secondary jet meets this criterion, the event is classified as a "dijet" event; two secondary jets meeting the criterion is a "trijet" event. If only the leading jet meets it, the event is a "monojet."

We are now in a position to implement the UA1 cuts. If any of the conditions below are met, the event would be excluded:

$$E_T^{miss} < 15 \text{ GeV}, \tag{5.12}$$

$$E_T^{miss} < 4\sigma, \tag{5.13}$$

where

$$\sigma \equiv 0.7\sqrt{E_T \text{ (total)}}, \tag{5.14}$$

$$|\text{angle}(\boldsymbol{p}_T^{miss}, \text{vertical})| < 20°, \tag{5.15}$$

$$|\eta^{jet(1)}| > 2.5. \tag{5.16}$$

The purpose of cuts (5.12) and (5.13) is to eliminate missing transverse energy events due to mismeasurement in the calorimetry.

Two further cuts (used first with the 1984 data) are especially helpful for eliminating events resulting from mismeasurement of QCD two-jet events. These cuts, however, use a less restrictive definition of jets (so that they can be applied to monojets as well as dijets):

$$E_T^{jet} \geqslant 8 \text{ GeV}. \tag{5.17}$$

(We caution the reader that eq. (5.17) is only used in conjunction with the cuts shown below, eqs. (5.18), (5.19).) The cuts eliminate events with

$$\text{angle}(\boldsymbol{p}_{jet(2)}, -\boldsymbol{p}_{jet(1)}) < 30°, \tag{5.18}$$

$$\text{angle}(\boldsymbol{p}_{jet(2)}, \boldsymbol{p}_T^{miss}) < 30°. \tag{5.19}$$

Although these cuts are helpful in removing QCD background, they can also be quite effective in removing monojets and dijets of supersymmetric origin.

We now describe the conditions which can trigger an event. The UA1 triggers are *less* efficient at measuring jet momenta than is the detector as described above. Furthermore the resolution is not as good either. Therefore, in testing whether our events pass the UA1 jet triggers, we further reduce the jet momenta by 20% (again 20% is UA1's best estimate [48]). After the reduction, we account for non-zero resolution of the jet trigger by smearing the resulting momentum according to the distribution:

$$e^{-(\delta p_J)^2/2\sigma_J^2}, \qquad \sigma_J = 0.2 p_J. \tag{5.20}$$

The final jet momentum thus obtained is used only to determine whether the given event passes the UA1 trigger. For other computations, the jet momentum before this last reduction and smear is used.

There were three UA1 triggers in the 1984 run. Events were kept if they satisfied any of the following conditions (where jet(1) is the jet with the highest E_T after smearing) [49]:

(i) $$E_T(\text{jet } 1) > 25 \text{ GeV} \quad (85\% \text{ run}), \tag{5.21}$$

$$E_T(\text{jet } 1) > 30 \text{ GeV} \quad (15\% \text{ run}); \tag{5.22}$$

(ii) $$E_T(\text{jet } 1) > 15 \text{ GeV},$$

$$|E_T^{\text{miss}} \text{ (left-hemisphere)} - E_T^{\text{miss}} \text{ (right-hemisphere)}| > 17 \text{ GeV}; \tag{5.23}$$

(iii) $$E_T \text{ (total in } |\eta| < 1.4) > 80 \text{ GeV}. \tag{5.24}$$

This last trigger requires a more restrictive η region than that used for other cuts and triggers ($|\eta| < 2.5$). To implement this particular trigger, we parameterized the data in the lower plot shown in fig. 3. This resulting distribution was scaled up by the same factor (1.67) as described in sect. 4. See discussion above eq. (4.7).

The second trigger (5.23) was not used for the 1983 run. While it apparently allows relatively few extra events from QCD sources, we found that it would allow an order-of-magnitude more events from supersymmetric sources if the gluino is quite light ($M(\tilde{g}) \lesssim 10$ GeV).

6. Sensitivities to assumptions and approximations

Having completed the discussion of our procedure, there are several questions concerning the sensitivity of our results to our assumptions. In which cases are we sensitive to the details of our smearing procedure?. First let us consider the case of a very light gluino.

By examining fig. 4 one can see why processes such as $\tilde{g}\tilde{g}$ where $M_{\tilde{g}}$ is small can have large uncertainties. The peak in the curve at low E_T^{miss} occurs where it does only because of the imposed cuts and triggers. Otherwise the true peak would occur at extremely low E_T^{miss}. The observable monojets are therefore very far out on the tail of this distribution. Because of the steeply falling curves, any smearing due to resolution and any mismeasurement due to inefficiencies can and do have large effects. These cannot be perfectly determined.

By contrast, when heavy particles are involved such as for the $\tilde{q}\tilde{g}$ process in fig. 4 or $\tilde{q}\bar{\tilde{q}}$ in fig. 5, then most events occur at E_T^{miss} and E_T^{jet} above the cuts and triggers so that the shapes of distributions are only mildly affected by cuts, and changes in the rates are not important. As a result our calculations are much more accurate

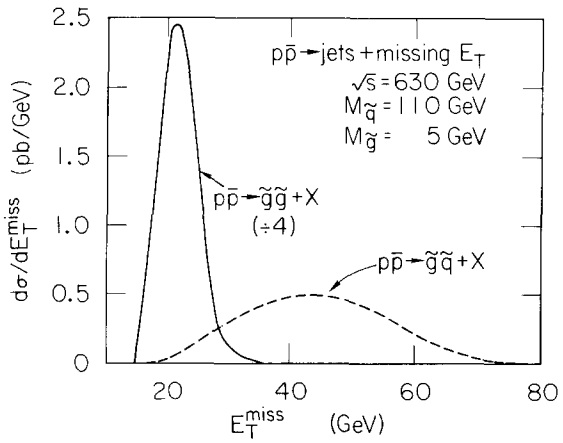

Fig. 4. The E_T^{miss} distribution expected from $\tilde{g}\tilde{g}$ (solid curve) and from $\tilde{q}\tilde{g}$ (dashed curve) production at $\sqrt{s} = 630$ GeV if $M_{\tilde{g}} = 5$ GeV and $M_{\tilde{q}} = 110$ GeV. The $\tilde{g}\tilde{g}$ distribution is cut off at small E_T^{miss} by experimental cuts. All of the new 1984 UA1 cuts and triggers are included.

when heavy particles are involved, and their reliability is limited primarily by the accuracy of perturbative QCD.

As a result of these observations, in the light gluino case, small changes in our procedures can result in a significant change in the number of events which pass the cuts. For example, we tried various other approaches to smearing. In applying conditions (5.12)–(5.14), our original procedure involved computing precisely E_T^{miss}

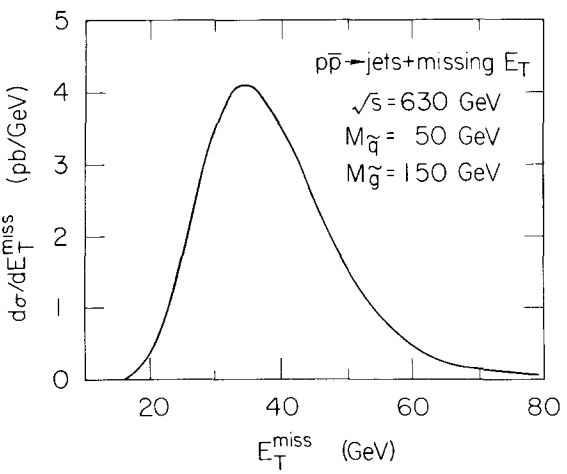

Fig. 5. The E_T^{miss} distribution expected from $\tilde{q}\tilde{q}$ production at $\sqrt{s} = 630$ GeV if $M_{\tilde{q}} = 50$ GeV and $M_{\tilde{g}} = 150$ GeV. All of the new 1984 UA1 cuts and triggers [23] are included.

and E_T (total) $\equiv E_T$ (jets) + E_T (remainder) from the knowledge of the various jet transverse energies which were smeared. Alternatively, one could first compute E_T^{miss} and E_T (jets) from unsmeared quantities and then smear the results. Similar remarks apply to the application of the jet trigger (eqs. (5.23) and (5.24)). We found that the results of these variations could affect the number of events passing the cuts by a factor of two if the gluino were light. For heavier gluinos (and scalar quarks), the sensitivity to the method of smearing was negligible.

For light gluinos our lack of precise knowledge of the excess or remainder transverse energy in an event (see eq. (4.9) and the discussion in sect. 4) contributes significantly to the uncertainty. This is again due to being on the tail of the E_T^{miss} distribution. Since we make the cut of eq. (5.13), $E_T^{miss} > 4\sigma$, where σ involves knowledge of this remainder energy, one is very sensitive to the remainder since it is a small fraction of the events which pass the cut. When gluino or scalar quark masses are sufficiently large, most events do pass the cut so we then have very little sensitivity to our choice of a distribution of remainder energies.

Another example of an uncertainty which is important for light gluinos but negligible for heavy gluinos and scalar quarks is that due to fragmentation effects. Altarelli et al. [22] have shown that different choices for implementing fragmentation can lead to differences of a factor of 2 to 3.

Another question as to the reliability of our results concerns the effects of ignoring hadronization (our final-state quarks and gluons are not converted into hadronic jets). In general, for the rates and distributions we discuss, we believe this approximation does not have major consequences. Ellis and Kowalski [16] who have studied this question also reached this conclusion. However, by ignoring hadronization, we are unable to calculate a number of interesting properties of the events; such as jet shapes, jet multiplicities, and jet invariant mass. In fact, the lack of hadronization means that when no coalescing occurs, the jets have zero invariant mass, which is a very crude approximation to the actual physical situation. However, when coalescing does occur (which is often necessary to pass cuts and triggers), then the invariant mass found for a coalesced jet is a reasonable approximation to the observable mass.

Hadronization is just one of a number of sources of uncertainty in the calculation of the dijet to monojet ratio. First, one should note that many of the observed monojet events have secondary jets with $E_T^{jet} = 6$–11 GeV. This is virtually always the case with events generated by our supersymmetry Monte Carlo. As a result the difference between monojets and dijets is a subtle one, quite subject to theoretical uncertainties.

Among the uncertainties are nonperturbative QCD corrections and spectator activity which can add to jet momenta, and energy leaving the jet cone (e.g., by gluon bremsstrahlung) which is not included in the definition of the jet. When gluinos or scalar quarks fragment, it is not known what fraction of the gluons goes outside the jet cone and what fraction adds to the jet energy. Gluon radiation by the hard jet will occasionally cause a monojet to fall below the trigger requirements.

Gluon radiation from a hard jet or other sources (which might or might not coalesce with a soft secondary jet) can sometimes lead to a secondary jet with $E_{\mathrm{T}}^{\mathrm{jet}} \geqslant 12$ GeV (we might call these dijets events "closet monojets"). We know that W and Z production often has an accompanying hadronic jet. Experimental resolution and efficiency also play an important role in determining the dijet to monojet ratio.

We believe that it is best to combine all missing energy events (monojets, dijets, trijets) and thereby increase the statistical significance while decreasing the sensitivity to theoretical and experimental limitations. However, this does not mean that one should ignore the monojet-dijet distinction. There is a great deal of information to be gained by considering them separately as will be seen when we discuss our results.

Finally, while a theorist can make every effort to model experimental conditions and while such efforts provide a great deal of insight, the final analysis will be done with a true detector simulation by the experimentalists. However, even detector simulation is not perfect since one never fully knows a detector.

7. Results for monojets and missing-energy events

7.1. RECAPITULATION

Our results are the consequence of the full analysis described in previous sections. All supersymmetric processes for the production of scalar quarks and gluinos were calculated along with all possible decay channels, and in the end they were summed. Our quoted cross section rates reflect this summation.

We report here rates for all combinations of $M_{\tilde{\mathrm{g}}}$ and $M_{\tilde{\mathrm{q}}}$. Detailed modeling of the new 1984 UA1 cuts and triggers is incorporated together with simulation of some detector resolutions and efficiencies (see sect. 5). Among the cuts are those which eliminate "back-to-back" events. Fragmentation and gluon bremsstrahlung were accounted for, although we do not hadronize our jets. Since the p_{T} distributions of initial-state parton distributions are not generally well-known and since our results show little sensitivity to different choices, we have chosen p_{T} (initial-state) $= 0$ here. And finally, the integrations were done by Monte Carlo techniques, but there were a variety of analytic checks for every process.

7.2. THE 1984 DATA

Let us first summarize the newly reported 1984 data from the UA1 Collaboration [23]. They found 23 monojets with at least 15 GeV of missing transverse energy in their 1984 run. They identified 9 as having the characteristics of the $\mathrm{W} \to \tau\nu$ ($\tau \to \nu +$ hadrons) source. Of the remaining 14 events, UA1 estimates that 6–8 events are due to background sources. We will take 13 events as the 90% confidence limit for the number of events which *could* represent new physics. Since their integrated luminosity in 1984 was about 270 nb^{-1}, the 90% confidence upper limit

for monojet production due to new physics is then 4.8 events/100 nb^{-1}. This is actually quite conservative since (as discussed below) our distributions show that most of these events are unlikely to be from supersymmetric sources so that the real limit might be as low as perhaps 2 events/100 nb^{-1}.

As discussed in sect. 6, theoretical calculations of monojet rates are subject to the fine distinction between monojets and dijets. We advocate use of the combined monojet + dijet + multijet rate. The UA1 Collaboration reports that after the back-to-back cuts, 2 dijet and no multijet events remain from the 1984 run where they estimate backgrounds at 2 events. The total number of missing-energy events (after τ subtraction) is then 16 with backgrounds at 8–10 events. We again take 13 events to be the 90% confidence level limit giving the limit for the rate of missing-energy events with $E_T^{miss} > 15$ GeV to be 4.8 events/100 nb^{-1}, while the *dijet* rate's limit is 2 events/100 nb^{-1}.

As we advocated in our previous paper [19], one can make a higher cut on E_T^{miss} in order to eliminate most backgrounds. Of the reported missing-energy events in the 1984 run, only 6 would pass an $E_T^{miss} > 40$ GeV cut. If we assume a background of 2 events, this leads to 8 events at the 90% confidence level or 3 events/100 nb^{-1}.

7.3. LIMITS ON SCALAR-QUARK AND GLUINO MASSES

Our results are summarized in the contour plots, figs. 6–9. They should only be compared with the 1984 UA1 data. Let us momentarily ignore the region at very low gluino masses where rates are low due to fragmentation effects. From fig. 6 showing the monojet rate for $E_T^{miss} > 15$ GeV and the data described above, we set the limits $M_{\tilde{q}} > 50$–60 GeV depending on $M_{\tilde{g}}$ and $M_{\tilde{g}} > 45$–55 GeV depending on $M_{\tilde{q}}$.

We advocate use of all missing-energy events as in fig. 7. From this plot and the above data, we find $M_{\tilde{q}} > 60$–70 GeV depending on $M_{\tilde{g}}$ and $M_{\tilde{g}} > 50$–70 GeV depending on $M_{\tilde{q}}$. This significant improvement in the limits occurs because, for these large masses, supersymmetry predicts that dijet production should dominate over monojet production even with the back-to-back cuts. So these results combining all missing-energy events are both more limiting and more reliable (since they need make no distinction among numbers of jets).

If one wishes instead to assume that we can accurately separate monojets and dijets, then the above results suggest that it will be useful to examine the dijet rate separately. This is, in effect, done by subtracting fig. 6 from fig. 7. Using the above data we then find

$$M_{\tilde{q}} > \begin{cases} 65, & M_{\tilde{g}} \approx 150 \text{ GeV} \\ 75, & M_{\tilde{g}} \approx 80 \text{ GeV}, \end{cases}$$

$$M_{\tilde{g}} > \begin{cases} 60, & M_{\tilde{q}} \approx 100 \text{ GeV} \\ 70, & M_{\tilde{q}} \approx 80 \text{ GeV}. \end{cases} \tag{7.1}$$

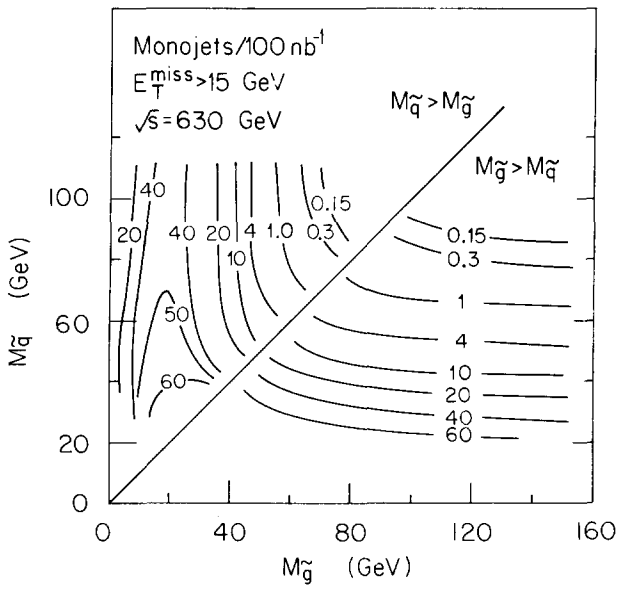

Fig. 6. The number of monojets per 100 nb^{-1} passing the new 1984 UA1 cuts and triggers [23] shown as a contour plot as a function of $M_{\tilde{g}}$ and $M_{\tilde{q}}$. The 1984 UA1 data have an integrated luminosity of about 270 nb^{-1}.

The limits quoted above would change by $\Delta M \approx 5$ GeV if our predictions were off by 50%.

If we turn to the event rate for $E_T^{miss} > 40$ GeV (figs. 8–9), we see that the limits are not as good for scalar quark masses and are non-existent for gluino masses. This occurs because the missing-energy events are predicted to be heavily populated in the $E_T^{miss} < 40$ GeV region (just as the backgrounds are). As gluino and scalar quark masses become very large, the distributions get quite hard, but there phase space cuts off the rate.

How precise should we treat the numbers we have obtained (shown on our contour plots, figs. 6–9)? There are a number of uncertainties which enter into our calculation, both from theoretical sources and experimental sources. Examples of the theoretical uncertainties are those associated with perturbative QCD discussed at the end of sect. 3. We have also stressed in sect. 6 that the uncertainties introduced due to our lack of knowledge of the transverse-energy distribution of the remainder, i.e., that part of an event not included in the observed jets. Other sources of uncertainty – smearing and our modeling of UA1 cuts and triggers were also discussed in sect. 6. In general, we expect the uncertainty in our numbers is less than a factor of two. This implies an uncertainty in our mass limits of roughly 5 GeV. However, in the particular ease where the gluino is light (say $M_{\tilde{g}} \lesssim 20$ GeV), much more care must be given to the estimation of uncertainties. In fact, the numbers

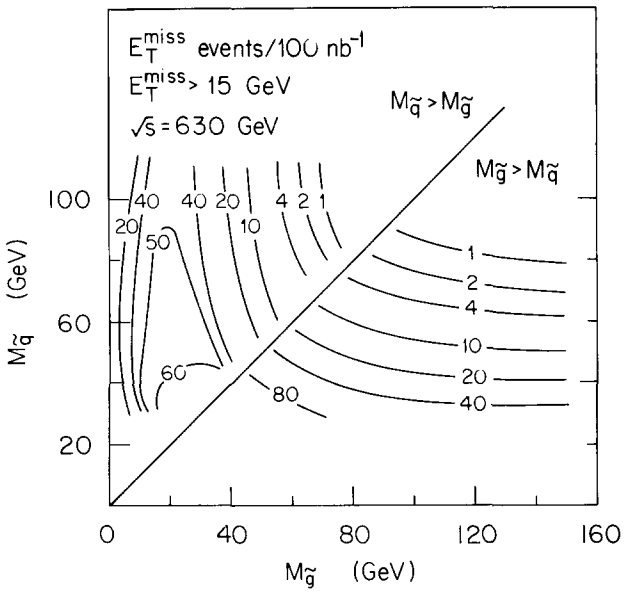

Fig. 7. The number of missing-energy events (monojets, dijets plus multijets) per 100 nb^{-1} passing the new 1984 UA1 cuts and triggers shown as a function of $M_{\tilde{g}}$ and $M_{\tilde{q}}$. The 1984 UA1 data have an integrated luminosity of about 270 nb^{-1}.

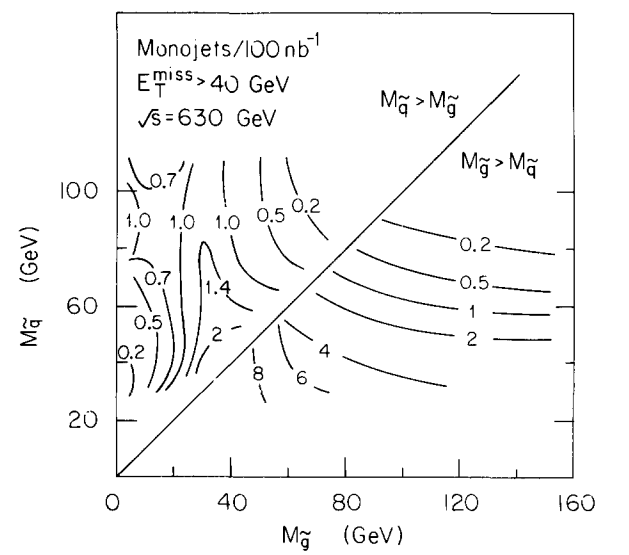

Fig. 8. The number of monojet events per 100 nb^{-1} as for fig. 6, but with the additional cut $E_T^{miss} > 40$ GeV imposed.

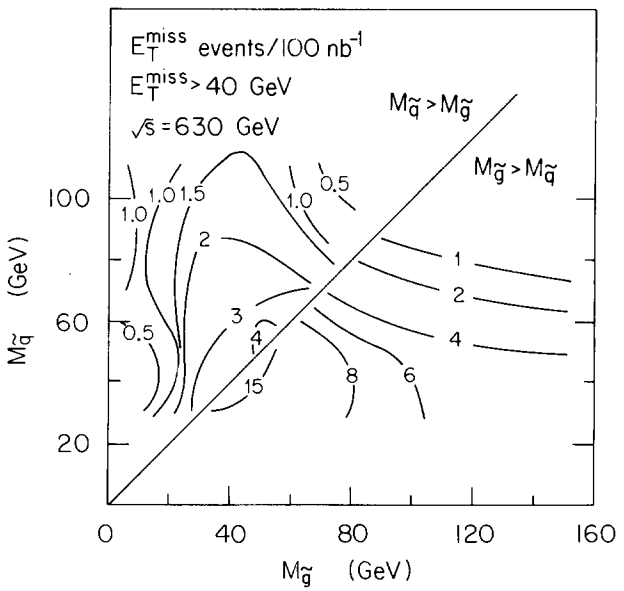

Fig. 9. The number of missing-energy events (monojets, dijets plus multijets) per 100 nb^{-1} as for fig. 7, but with the additional cut $E_T^{miss} > 40$ GeV imposed.

shown in our contour plots are much less certain in this regime. We now turn to the case of the light gluino in more detail.

7.4. ON THE QUESTION OF LIGHT GLUINOS

We have chosen to interpret the data in terms of limits. Before addressing the question of whether some of the observed events may actually be due to supersymmetry, it will be useful to return to the subject of the very light gluino. As is evident in figs. 6 and 7, the predicted event rates drop off as $M_{\tilde{g}}$ becomes very small. Very light gluinos lose much of their energy due to fragmentation and gluon bremsstrahlung, and therefore they lead to very little missing energy. As a result very few pass the E_T^{miss} cuts.

The calculations for very low mass gluinos are subject to much larger uncertainties due to fragmentation and to the surviving events being on the tails of the E_T^{miss} and E_T^{jet} distributions. We would predict for $M_{\tilde{q}} \approx 100$ GeV 26 events/100 nb^{-1} for a 5 GeV gluino and 13 events/100 nb^{-1} for a 3 GeV gluino (these are all monojets; dijet production is negligible). While these numbers are much larger than the 4.8 events limit, one cannot neglect the uncertainties intrinsic to theoretical calculations for light gluinos, discussed in sect. 6. Our tests convince us that these uncertainties could be as much as a factor of 4 or 5 if added linearly. In spite of this large uncertainty, our predicted event rate is large enough to conclude that $M_{\tilde{g}} = 5$ GeV is

ruled out and that $M_{\tilde{g}} = 3$ GeV is very marginal. If the photino mass is nonzero the photino would carry off even more energy, and our results would be strengthened.

An additional input on this subject comes from the beam-dump experiments. A recent BEBC experiment [39] gets the limits $M_{\tilde{g}} > 3$–4 GeV at the 90% confidence level (depending on the value of $M_{\tilde{q}}$). Therefore, what some authors have referred to as a "window" allowing light gluinos, is at best a "peep-hole," and most likely is ruled out.

This conclusion could not be reached in the papers (including ours) analyzing the 1983 data for two primary reasons. The new missing-energy trigger in the 1984 run is extremely important for $\tilde{g}\tilde{g}$ production when $M_{\tilde{g}} \lesssim 10$ GeV. It raises our predictions in this case by an order-of-magnitude, while experimentally this trigger does not dramatically change the observed rate. The calculation of the $\tilde{g}\tilde{g}g$ process by Herzog and Kunszt [36] was not available for the earlier analyses, and we find it increases our predictions for 5 GeV gluinos by a factor of 3. While other recent refinements bring down the rate a little, the end result is that because of the higher rates predicted, it is now possible (or almost possible) to rule out light gluinos.

7.5. SUPERSYMMETRY – LOST OR FOUND?

Could some of the observed monojet events be due to the production of gluinos or scalar quarks? The UA1 Collaboration [23] cannot rule out the possibility that 6–8 of the monojets come from new physics. There are, however, two factors which argue against the monojets coming from gluino or scalar quark production. Both are consequences of the fact that the appropriate event rate (2–3 monojets/100 nb^{-1}) only occurs for large $M_{\tilde{q}}$ or $M_{\tilde{g}}$ (≈ 60 GeV). For such masses we would predict 4–6 dijets/100 nb^{-1}, and these certainly have not been observed. Furthermore, at these masses one would expect significant numbers of monojets with $E_{\text{T}}^{\text{miss}} > 45$ GeV, and only one was observed in the 1984 run (compare fig. 5).

The two observed dijet events (surviving the back-to-back cuts) in the 1984 run have $E_{\text{T}}^{\text{miss}} \geqslant 55$ GeV. Although there is a roughly equal background expected, these backgrounds are unlikely to have so much $E_{\text{T}}^{\text{miss}}$. A 70–90 GeV scalar quark could give dijets with such characteristics and with this rate, and would produce very few monojets. Clearly, however, such speculation must await considerably more statistics.

7.6. COMMENTS ON BACKGROUNDS

Some if not all of the observed monojet events must be due to "backgrounds," i.e., due to standard model physics. One can produce c, b and t pairs through the usual QCD processes, and their semileptonic decays will occasionally mimic monojets. Monojets can also arise from a variety of processes in which a $\text{W}^{\pm}$ or Z^0 boson is produced. Depending on the process, there may be a hard gluon (jet) produced in

conjunction with the $W^{\pm}$ or Z^0. The most common process is, of course, $W \to \tau\nu$ with $\tau \to \nu +$ hadrons. The reaction $p\bar{p} \to Z^0 + g$ with $Z^0 \to \nu\bar{\nu}$ also is important. We have calculated these last two processes using the same procedures and analyses as described for supersymmetric processes. We consider our results which are consistent with those reported by the UA1 Collaboration [14,23] and other theoretical calculations [50] as another check of our analysis. Other monojets could come from $W^{\pm} \to c\bar{s}$, $t\bar{b}$, $e\nu$, $\mu\nu$ and $\tau\nu$ (with $\tau \to e\nu\nu$ or $\mu\nu\nu$). Still others come from $Z^0 \to \tau\tau$, $c\bar{c}$, $b\bar{b}$, and $t\bar{t}$. Eventually, when more data are accumulated, these background processes may be directly or indirectly measured.

8. Theoretical models and alternatives

8.1. IMPLICATIONS OF MINIMAL LOW-ENERGY SUPERGRAVITY MODELS

Throughout this paper, we have treated the gluino and scalar-quark masses as independent parameters. Furthermore, we took the photino to be the LSP and assumed that its mass could be neglected. If we are willing to adopt a particular approach to low-energy supergravity model building [8], we can constrain certain parts of the $M_{\tilde{q}} - M_{\tilde{g}}$ plane.

For illustration purposes, let us consider a class of models which have been often referred to as being "minimal" supergravity models [51–53]. These models are "minimal" in two respects. First, they consist of the minimal number of particles: the standard model particles with two Higgs doublet and their supersymmetric partners. Second, these models depend on a minimal set of parameters: the gravitino mass ($m_{3/2}$), the gluino mass ($M_{\tilde{g}}$), μ (a supersymmetric higgsino mass), A (a parameter related to the super-Higgs mechanism), and v_2/v_1 (the ratio of vacuum expectation values of the two Higgs fields). These models are obtained in two steps. First, starting with an $SU(3) \times SU(2) \times U(1)$ (or grand unified) gauge theory coupled to supergravity, an effective renormalizable field theory at the Planck mass (M_P) is obtained in the limit of $M_P \to \infty$. Second, renormalization group equations are used in order that we may obtain the effective low energy theory which is valid at the electroweak scale. It turns out that the effective theory at the Planck scale does not break the $SU(2) \times U(1)$ gauge symmetry. Thus, in order that the $SU(2) \times U(1)$ electroweak group be broken in the standard way in the low-energy effective theory (such that $SU(3)_{color} \times U(1)_{em}$ remain conserved), it must happen that the parameters of the theory, which evolve via the renormalization group, satisfy an appropriate set of conditions. These conditions are quite restrictive and tend to reduce much of the freedom in the choice of parameters of the model. For example, if we assume that $m_t \approx 40$ GeV (as may be indicated by recent results [54] of UA1), then it follows [52–53] that $v_1 \approx v_2$ and $B\mu m_{3/2} \sim O(m_{3/2}^2)$, where $B \equiv A - 1$ at the Planck scale and is a number of order unity. The renormalization group analysis of such

models has been performed, and the following results have been obtained:

$$M_{\tilde{\gamma}} \approx \tfrac{1}{6} M_{\tilde{g}}\,, \tag{8.1}$$

$$M^2_{\tilde{q}_L} = m^2_{3/2} + C_{\tilde{q}_L} M^2_{\tilde{g}} + m^2_Z \left(T_{3q} - e_q \sin^2\theta_W\right)\cos 2\beta\,, \tag{8.2}$$

$$M^2_{\tilde{q}_R} = m^2_{3/2} + C_{\tilde{q}_R} M^2_{\tilde{g}} + m^2_Z e_q \sin^2\theta_W \cos 2\beta\,, \tag{8.3}$$

$$M^2_{\tilde{\ell}_L} = m^2_{3/2} + C_{\tilde{\ell}_L} M^2_{\tilde{g}} + m^2_Z \left(T_{3\ell} - e_\ell \sin^2\theta_W\right)\cos 2\beta\,, \tag{8.4}$$

$$M^2_{\tilde{\ell}_R} = m^2_{3/2} + C_{\tilde{\ell}_R} M^2_{\tilde{g}} + m^2_Z e_\ell \sin^2\theta_W \cos 2\beta\,, \tag{8.5}$$

where $\tan\beta \equiv v_2/v_1$ and the constants are given by: $C_{\tilde{q}_L} = 0.85$, $C_{\tilde{q}_R} = 0.78$, $C_{\tilde{\ell}_L} = 0.08$, and $C_{\tilde{\ell}_R} = 0.02$. T_{3i} and e_i $(i = q, \ell)$ are the weak isospin and electric charge (in units of e) of the quarks and leptons respectively. Strictly speaking, eqs. (8.2) and (8.3) must be modified somewhat for the third generation; we refer the reader to ref. [53] for the details. Eq. (8.1) follows from eq. (2.1); in models where the gluino mass is not too large, the LSP is approximately a pure photino with the mass shown above. We noted above that in models where m_t is not too heavy, it follows that $v_1 \approx v_2$. This in turn implies that $\cos 2\beta \approx 0$ and therefore the scalar-quark and scalar-lepton masses depend on two parameters. It follows that

$$M^2_{\tilde{\ell}_R} \approx M^2_{\tilde{q}} - 0.8\, M^2_{\tilde{g}}\,. \tag{8.6}$$

This is an interesting constraint, in that it implies that the gluino cannot be much heavier than the scalar quark.

Another constraint can be obtained by considering the cosmological implications of a light photino [55–56]. In particular, since photinos are the LSP (and thus stable), their annihilation rate must be sufficiently efficient to reduce their abundance in the early universe to a cosmologically acceptable level. (Another cosmologically acceptable solution – to have the photino nearly massless like the neutrino – is unacceptable, since by eq. (8.1), it would imply a nearly massless gluino, which is almost certainly ruled out.) A calculation of Ellis et al. [56] shows that $M_{\tilde{\gamma}} \gtrsim 0.5$ GeV if $M_{\tilde{q}} \gtrsim 20$ GeV and $M_{\tilde{\gamma}} \gtrsim 5$ GeV if $M_{\tilde{q}} \gtrsim 100$ GeV. (The efficiency of photino annihilation decreases as the scalar-quark mass increases.) Using eq. (8.1), this leads to a lower limit on the gluino mass as a function of the scalar-quark mass.

The two constraints discussed above substantially limit the region of the $M_{\tilde{q}} - M_{\tilde{g}}$ plane which is consistent with the minimal low-energy supergravity model described above [57].

8.2. AN ALTERNATIVE: THE LIGHT HIGGSINO

It would be misleading to finish the discussion of low-energy supergravity models without indicating the possibility of other scenarios. We have emphasized earlier that many of our conclusions (and our strict mass limits) depend on the assumption that the photino is the LSP. It is of interest to consider whether it is possible to construct models where this assumption is not valid and what the implications are for another candidate for the LSP.

We will consider the case where the LSP is a light higgsino. In the minimal model discussed above, the higgsino mass turns out to be $M_{\tilde{H}} \sim \mu \sim O(m_{3/2})$. Hence, unless the gluino mass is large enough (implying a large value for $M_{\tilde{\gamma}}$ via eq. (8.1)), the higgsino will not be the LSP. However, as shown in ref. [27], one can easily generalize the minimal model in such a way that the parameter μ is not constrained to be $O(m_{3/2})$. In such a model, the higgsino will be the LSP as long as $\mu < M_{\tilde{\gamma}}$.

Let us summarize some of the phenomenological implications of this alternative scenario. First, the photino will tend to be the second lightest supersymmetric particle, and hence only two decay channels are available: $\tilde{\gamma} \to f\bar{f}\tilde{H}$ or $\tilde{\gamma} \to \gamma\tilde{H}$. The latter decay occurs via a one-loop Feynman diagram (see refs. [27] and [28]). The three-body tree-level decay of the photino occurs via the exchange of a virtual $\tilde{f}$. Because the $\tilde{H}f\tilde{f}$ vertex is proportional to the mass of the *fermion* (m_f), this decay rate is negligible and the decay $\tilde{\gamma} \to \gamma\tilde{H}$ is the dominant one. Calculations of the two-body decay yield approximately:

$$\tau_{\tilde{\gamma}} \approx 10^{-11}\ \text{sec} \left(\frac{1\ \text{GeV}}{M_{\tilde{\gamma}}} \right)^3 , \tag{8.7}$$

which indicates that the photino decay is prompt unless $M_{\tilde{\gamma}}$ is sufficiently light. Note that because the photino is now unstable, the cosmological limits for the photino obtained by Ellis et al. [56] no longer apply. Instead, one now finds cosmological limits on the higgsino mass: either $M_{\tilde{H}} \lesssim 100$ eV or $M_{\tilde{H}} \gtrsim m_b$. Since the higgsino and gluino masses are logically independent, there is no phenomenological reason which rules out a massless higgsino.

Scalar-quark and gluino decays are, however, unchanged. In principle, one could have $\tilde{g} \to q\bar{q}\tilde{H}$ and $\tilde{q} \to q\tilde{H}$. However, as stated above, the $\tilde{H}f\tilde{f}$ vertex is proportional to m_f and hence these decay rates can be neglected as compared with the standard ones involving the photino. Two cases can be envisioned. If the photino is long lived (see eq. (8.7)), then it will escape the collider detectors, and there is no change in any of the results obtained in this paper. However, if the photino decays promptly, $\tilde{\gamma} \to \gamma\tilde{H}$, then the phenomenology changes drastically. First, when supersymmetric particles are produced, the resulting missing-energy spectrum softens considerably.

As a result, fewer events pass the UA1 E_T^{miss} cuts, and the limits on supersymmetric masses obtained in sect. 7 are significantly weakened. Although we have not yet implemented this possibility in our Monte Carlo program, we may quickly obtain an estimate as to the new limits. We do this by noting that Dawson [30] has investigated the implication of missing energy events for supersymmetric models which violate R-parity. In these models, the photino is the LSP but is unstable and decays via $\tilde{\gamma} \to \gamma\nu$. Thus, the signature is identical to the case we are considering here, so we may use her results. Dawson finds (see fig. 11 of ref. [30]) that the number of events which pass the UA1 cuts and triggers is roughly a factor of five less than in the case of a stable photino. This suppression factor is roughly independent of $M_{\tilde{q}}$ and $M_{\tilde{g}}$. If we reduce the numbers which appear in figs. 6–9 by a factor of five, we would obtain the following allowed regions for $M_{\tilde{q}}$ and $M_{\tilde{g}}$:

$$M_{\tilde{g}} \lesssim 5 \text{ GeV} \quad \text{or} \quad M_{\tilde{g}} \gtrsim 40 \text{ GeV}, \tag{8.8a}$$

$$M_{\tilde{q}} \gtrsim 45\text{–}60 \text{ GeV}. \tag{8.8b}$$

In eq. (8.8b), the better limit is obtained as we take the gluino mass approaching the scalar-quark mass. Note that the "light-gluino window" has returned. That is, we no longer feel able to rule out gluino masses of order $3 \lesssim M_{\tilde{g}} \lesssim 5$ GeV since the number of predicted events passing the UA1 cuts has been significantly reduced.

Suppose we accept the possibility that a few of the monojets could be due to supersymmetry where the higgsino is the LSP. As argued above, when scalar quarks and gluinos are produced, they decay into photinos which subsequently decay into higgsinos: $\tilde{\gamma} \to \gamma\tilde{H}$. Thus, these events should contain photons! Can this be ruled out? At present, the answer seems to be negative. The photon could not be easily distinguished from a π^0 in the UA1 detector, so these events would just exhibit extra observed neutral energy. A signature which could confirm or exclude such a model is the presence of events where one photino gives a hard photon plus a soft $\tilde{H}$, and the other photino gives a soft photon and a hard $\tilde{H}$, so the full event has large E_T^{miss}, an isolated hard photon and one or more jets.

Note, however, that some limits do exist from e^+e^- physics. The process $e^+e^- \to \tilde{\gamma}\tilde{\gamma}$, $\tilde{\gamma} \to \gamma\tilde{H}$ can take place yielding $e^+e^- \to \gamma\gamma$ + missing energy. Such a process has been searched for at PETRA; no events of this type above background have been seen [58]. This implies that the cross section for $e^+e^- \to \tilde{\gamma}\tilde{\gamma}$ cannot be too large. Since this process occurs via exchange of a scalar electron, the absence of this process (assuming an unstable photino which decays radiatively) puts a limit on the scalar-electron: $M_{\tilde{e}} \gtrsim 100$ GeV. By eqs. (8.6), this implies that $M_{\tilde{q}} \gtrsim 100$ GeV. Thus, in the case where the higgsino is the LSP, supersymmetry cannot be the explanation for monojets unless the gluino is very light, $M_{\tilde{g}} \lesssim 5$ GeV.

9. Future tests and conclusions

9.1. SEARCH FOR SUPERSYMMETRY AT FUTURE HADRON COLLIDERS

What are the implications of our analyses for higher-energy colliders such as the Tevatron and the SSC? Experiments searching for supersymmetry or for other new physics will have to make choices on cuts and triggers, and will have somewhat different resolutions and efficiencies. The choices will be based in part on how backgrounds scale, but also on how quantities such as E_{r} scale (where E_{r} is the remaining transverse energy in an event after the jets are removed). Of course, E_{r} also depends on how the experiment chooses (or needs) to define the jets; both the jet algorithm and the required minimum $E_{\mathrm{T}}^{\mathrm{jet}}$ enter this definition. The theoretical calculation of E_{r} involves knowledge of initial-state radiation and other aspects which theorists are just now learning to include in QCD Monte Carlo programs.

As a result of our ignorance of backgrounds, of future experimental conditions and of the scaling of E_{r}, it will be difficult to make precise predictions for the Tevatron and the SSC. We do intend, however, to study these questions and to try to find some qualitative answers.

9.2. SUMMARY AND CONCLUSIONS

We wish now to summarize the results which we have described in this paper. Our analysis is based on the newly reported UA1 collaboration data [23] from the 1984 run with an integrated luminosity of approximately 270 nb^{-1}. Since somewhat different cuts and triggers were used than in the 1983 run and the energy is different, our results apply only to the 1984 data.

We conclude that if there is any excess of monojet events after backgrounds are subtracted, it is unlikely to come from the production of gluinos or scalar quarks, assuming the photino is the lightest supersymmetric particle. We showed that the combination of a powerful new trigger in the 1984 run and the inclusion of the $\tilde{g}\tilde{g}g$ process in the analysis, has reduced the so-called "window" for a light (~ 5 GeV) gluino to a "peep-hole" at most. For heavier gluons or scalar quarks (up to 60 GeV), the problem is that these strongly-interacting supersymmetric particles would have been produced at too large a rate (compared to what is observed). For even heavier gluinos or scalar quarks, where phase space would keep the rate down at appropriate levels, we find that the dijet-to-monojet ratio would be 2 or greater. With the UA1 back-to-back cuts imposed, only 2 dijet events survive (before background subtraction), so that at most one monojet would be expected. Furthermore, the $E_{\mathrm{T}}^{\mathrm{miss}}$ and $E_{\mathrm{T}}^{\mathrm{jet}}$ distributions for such masses would be significantly harder than what is observed experimentally (with poor statistics). So there appears to be no range of masses which would lead to the type and rate of monojet events observed from these sources.

The two dijet events observed in the 1984 run [23] have very large E_T^{miss}. These events are certainly consistent with the type and rates expected from, say, $\tilde{q}\tilde{q}$ production with $M_{\tilde{q}} = 70$–90 GeV and $M_{\tilde{g}}$ somewhat larger. However intriguing these two events are, there may be a long wait for adequate statistics to learn more about their origin.

What we can do is set lower limits on the masses of gluinos and scalar quarks. We have chosen to be conservative and to assume (for setting limits) that all missing-energy events above UA1 background estimates are due to supersymmetry. If we do this, we find that the lower limits (90% confidence level) on gluino masses are 60–70 GeV depending on scalar quark mass. The lower limits on scalar-quark masses are 65–75 GeV depending on gluino mass. These are the most restrictive limits found to date for any supersymmetric particle. Imperfections in our modeling of UA1 experimental conditions and uncertainties from nonperturbative QCD effects can change these numbers for limits by ± 5 GeV.

If we change one of our basic assumptions and assume that the Higgsino is the lightest supersymmetric particle, then our analysis changes somewhat. Because the photino would decay, the missing energy in events with gluinos and/or scalar quarks would be softened, implying that fewer events would pass the UA1 cuts and triggers. We find new mass limits which are less restrictive than those above: $M_{\tilde{g}} \lesssim 5$ GeV or $M_{\tilde{g}} \gtrsim 40$ GeV, and $M_{\tilde{q}} \gtrsim 45$–60 GeV. In particular the light gluino window has reappeared.

These new limits are effective in restricting some models for supersymmetry which were specially designed to produce low masses for some supersymmetric particles.

Although the mass limits we have found are quite large, note that we have yet to reach m_W. If supersymmetry is to explain the origin of the electroweak scale, then it is natural to assume that this is the relevant scale for determining the masses of certain supersymmetric particles. Thus, it certainly is not unreasonable to expect supersymmetric masses to be on the order of 100 GeV or perhaps somewhat larger. The fact that the CERN Collider has shown no evidence for supersymmetry to date is disappointing, but in no way should this be considered as a problem for the theory. In fact, based on our analysis, it is clear that the Tevatron (with its larger energy and luminosity anticipated) will have the capability of investigating a new range of masses of particular interest to supersymmetry.

We wish to acknowledge useful conversations with theoretical colleagues including G. Altarelli, R. Arnowitt, V. Barger, A. De Rújula, J. Ellis, S. Ellis, R. Field, J. Gunion, I. Hinchliffe, B. Humpert, Z. Kunszt, F. Paige, D. Soper, X. Tata, and F. Yndurain. We have benefited greatly from interactions with experimentalists from the UA2 collaboration including P. Darriulat and from the UA1 collaboration including R. Batley, K. Eggert, A. Honma, A. Kernan, W. Kozanecki, F. Pauss, E. Radermacher, J. Rohlf, C. Rubbia, A. Savoy-Navarro, D. Smith, and C. Tao.

Appendix A

MATRIX ELEMENTS OF SUPERSYMMETRIC PROCESSES

We have computed the squared matrix elements for the supersymmetric processes given by eqs. (3.9)–(3.14), (3.17) and (3.18). Many of these can be found in the literature (see e.g., refs. [11,13]). For convenience, we have collected the necessary formulas here. Our notation is as follows: $|\tilde{\mathfrak{M}}|^2_{\text{ave}}$ is the squared matrix element summed over final state spins and colors and averaged over initial state spins and colors. We do *not* include a factor of $\frac{1}{2}$ if there are two identical particles in the final state in the formulas below. However, such a factor must be included if a total cross section is computed by integrating over the full 4π steradians. A few comments on each calculation are provided.

A.1. Gluino Pair Production.

(i) $gg \to \tilde{g}\tilde{g}$ (fig. 10a)

$$|\tilde{\mathfrak{M}}(gg \to \tilde{g}\tilde{g})|^2_{\text{ave}}$$

$$= \frac{9g_s^4}{4}\left\{\frac{2\left(M_{\tilde{g}}^2 - t\right)\left(M_{\tilde{g}}^2 - u\right)}{s^2} + \frac{M_{\tilde{g}}^2\left(s - 4M_{\tilde{g}}^2\right)}{\left(t - M_{\tilde{g}}^2\right)\left(u - M_{\tilde{g}}^2\right)} + f(t,u) + f(u,t)\right\}, \tag{A.1}$$

where the function $f(t,u)$ is given by:

$$f(t,u) = \frac{\left(M_{\tilde{g}}^2 - t\right)\left(M_{\tilde{g}}^2 - u\right) - 2M_{\tilde{g}}^2\left(M_{\tilde{g}}^2 + t\right)}{\left(t - M_{\tilde{g}}^2\right)^2}$$

$$+ \frac{\left(M_{\tilde{g}}^2 - t\right)\left(M_{\tilde{g}}^2 - u\right) + M_{\tilde{g}}^2(u - t)}{s\left(t - M_{\tilde{g}}^2\right)}. \tag{A.2}$$

In computing this amplitude, we have employed the trick which Georgi et al. [59] used to compute the squared matrix element for $gg \to c\bar{c}$. By setting $p_1 \cdot \varepsilon(p_1) = p_2 \cdot \varepsilon(p_2) = 0$ directly in the amplitude for fig. 10a (where p_i and $\varepsilon(p_i)$ are the four-momenta and polarization vectors of the initial gluons), one can show that it is then correct to replace $\Sigma_\lambda \varepsilon^\mu_\lambda(p_i)\varepsilon^\nu_\lambda(p_i)^* \to -g^{\mu\nu}$ for *both* initial gluons.

(ii) $q\bar{q} \to \tilde{g}\tilde{g}$ (fig. 10b)

$$|\overline{\mathcal{M}}(q\bar{q} \to \tilde{g}\tilde{g})|^2 = \frac{8g_s^4}{27}\left\{\frac{9\left[\left(M_{\tilde{g}}^2 - t\right)^2 + \left(M_{\tilde{g}}^2 - u\right)^2 + 2M_{\tilde{g}}^2 s\right]}{s^2}\right.$$

$$\left. + \frac{M_{\tilde{g}}^2 s}{\left(t - M_{\tilde{q}}^2\right)\left(u - M_{\tilde{q}}^2\right)} + g(t,u) + g(u,t)\right\}, \quad \text{(A.3)}$$

where

$$g(t,u) = 4\left(\frac{M_{\tilde{g}}^2 - t}{M_{\tilde{q}}^2 - t}\right)^2 + \frac{9\left[\left(M_{\tilde{g}}^2 - t\right)^2 + M_{\tilde{g}}^2 s\right]}{s\left(t - M_{\tilde{q}}^2\right)}. \quad \text{(A.4)}$$

In the above equations, we have summed over $\tilde{q}_L$ and $\tilde{q}_R$ exchange (for fixed initial flavor q). We have taken $\tilde{q}_L$ and $\tilde{q}_R$ to be degenerate in mass which we denote by $M_{\tilde{q}}$.

The one subtlety in computing this process is the sign of the interference terms. To get these signs correctly, note that there is a relative minus sign between the second and third graphs of fig. 10b. This sign arises due to Fermi statistics in the interchange of identical final-state gluino lines. In addition there is a relative minus

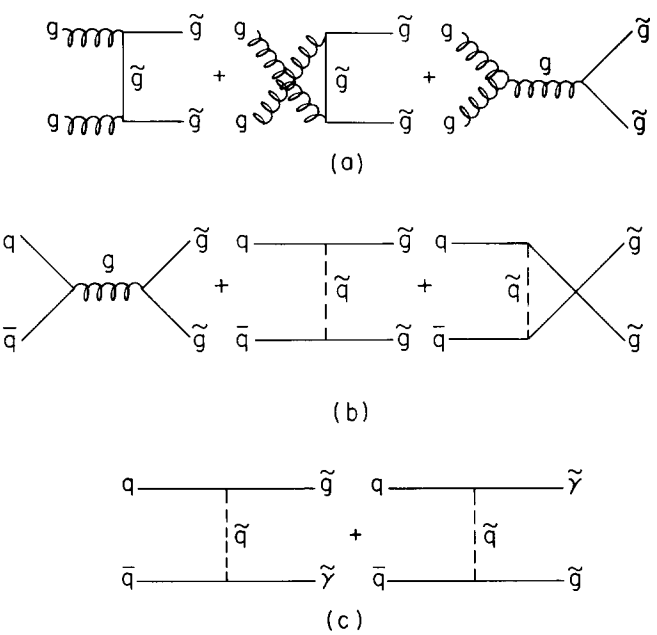

Fig. 10. Graphs for the production of gluinos. Graphs (a) and (b) show $\tilde{g}\tilde{g}$ production via gg and $q\bar{q}$ scattering respectively. Graph (c) shows $\tilde{g}\tilde{\gamma}$ production via $q\bar{q}$ scattering. For $\tilde{g}\tilde{q}$ production, see fig. 11.

sign between the first two graphs shown in fig. 10b. This sign is a little more subtle, although it can be traced to the fact that all fermion fields anticommute. This sign is analogous to the one which appears in the s-t channel interference in $e^+e^- \to e^+e^-$.

A.2. $qg \to \tilde{q}\tilde{g}$ *(fig. 11d).*

$$|\tilde{\mathcal{M}}(qg \to \tilde{q}\tilde{g})|^2_{ave}$$

$$= g_s^4 \left\{ \frac{4\left(M_{\tilde{g}}^2 - u\right)}{9s} - \frac{8M_{\tilde{q}}^2\left(M_{\tilde{g}}^2 - t\right)}{9\left(t - M_{\tilde{q}}^2\right)^2} + \frac{s\left(M_{\tilde{g}}^2 - u\right) + 2M_{\tilde{g}}^2\left(M_{\tilde{q}}^2 - u\right)}{\left(u - M_{\tilde{g}}^2\right)^2} \right.$$

$$+ \frac{tM_{\tilde{q}}^2 - uM_{\tilde{g}}^2}{\left(u - M_{\tilde{g}}^2\right)\left(t - M_{\tilde{q}}^2\right)} + \frac{4M_{\tilde{q}}^2M_{\tilde{g}}^2 - tM_{\tilde{q}}^2 - uM_{\tilde{g}}^2}{18s\left(t - M_{\tilde{q}}^2\right)}$$

$$\left. + \frac{M_{\tilde{g}}^2 s - \left(u - M_{\tilde{q}}^2\right)\left(s - M_{\tilde{q}}^2 + M_{\tilde{g}}^2\right)}{s\left(u - M_{\tilde{g}}^2\right)} \right\}. \tag{A.5}$$

This amplitude can be written in many different ways (using $s + t + u = M_{\tilde{q}}^2 + M_{\tilde{g}}^2$). We have checked that the above form is identical to the more complicated looking form given in ref. [11]. Our definitions here are: $t = (p_1 - k_1)^2$, $u = (p_1 - k_2)^2$ where the four momenta are chosen as indicated in parentheses: $g(p_1) + q(p_2) \to \tilde{q}(k_1) + \tilde{g}(k_2)$.

A.3. Scalar-Quark Pair Production. In the formulas given below, we take $\tilde{q}_L$ and $\tilde{q}_R$ to be degenerate in mass and we sum over the production of both types of scalar quarks. In addition, we assume that n_f flavors of scalar quarks are degenerate and sum over the production of all possible flavors when appropriate. In this paper, we have taken $n_f = 5$.

(i) $gg \to \tilde{q}\bar{\tilde{q}}$ (fig. 11a)

$$|\tilde{\mathcal{M}}(gg \to \tilde{q}\bar{\tilde{q}})|^2_{ave} = \frac{n_f g_s^4}{192} \left\{ 56 - \frac{2\left(4M_{\tilde{q}}^2 - s\right)^2}{\left(t - M_{\tilde{q}}^2\right)\left(u - M_{\tilde{q}}^2\right)} \right.$$

$$\left. + \frac{9}{s^2}\left[8s\left(4M_{\tilde{q}}^2 - s\right) + (u - t)^2\right] + h(t, u) + h(u, t) \right\}, \tag{A.6}$$

where

$$h(t, u) = 32\left(\frac{t + M_{\tilde{q}}^2}{t - M_{\tilde{q}}^2}\right)^2 + \frac{7\left(s - 4t - 4M_{\tilde{q}}^2\right)}{t - M_{\tilde{q}}^2}$$

$$+ \frac{6\left[(t - u)\left(s - 4t - 4M_{\tilde{q}}^2\right) - 2\left(M_{\tilde{q}}^2 - u\right)\left(s - 2t - 6M_{\tilde{q}}^2\right)\right]}{s\left(t - M_{\tilde{q}}^2\right)}. \tag{A.7}$$

This result has been obtained from ref. [11].

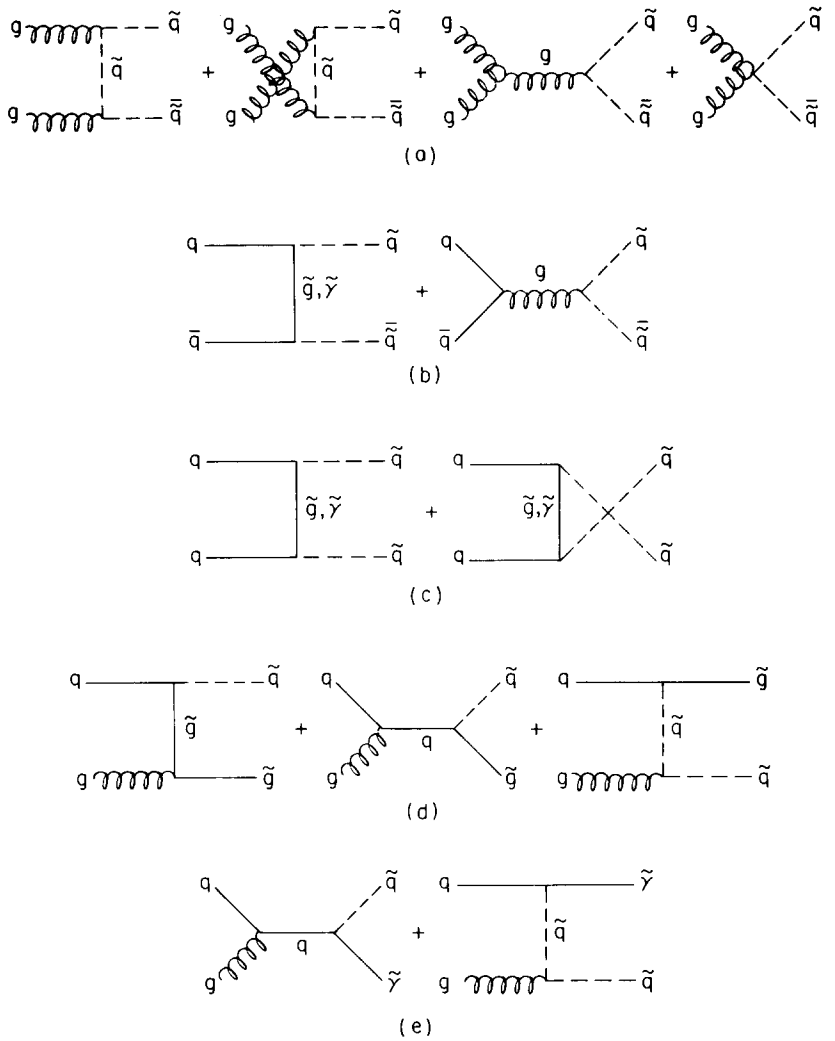

Fig. 11. Graphs for the production of scalar quarks. Graphs (a) and (c) show $\tilde{q}\tilde{q}$ production via gg and qq scattering respectively while (b) shows $\tilde{q}\bar{\tilde{q}}$ production. See also fig. 12. $\tilde{g}\tilde{q}$ and $\tilde{\gamma}\tilde{q}$ production are shown in graphs (d) and (e) respectively.

(ii) $q_i q_j \to \tilde{q}_i \tilde{q}_j$ (fig. 11c). If $i \neq j$, then

$$|\bar{\mathcal{M}}(q_i q_j \to \tilde{q}_i \tilde{q}_j)|^2_{\text{ave}} = \tfrac{4}{9} g_s^4 k(t,u), \tag{A.8}$$

where

$$k(t,u) = \frac{sM_{\tilde{g}}^2 + tu - M_{\tilde{q}}^4}{\left(t - M_{\tilde{g}}^2\right)^2}, \tag{A.9}$$

where we have summed over degenerate $\tilde{q}_L$ and $\tilde{q}_R$ but take the flavors i and j to be fixed. An identical formula holds for $\bar{q}_i\bar{q}_j \to \bar{\tilde{q}}_i\bar{\tilde{q}}_j$ and $q_i\bar{q}_j \to \tilde{q}_i\bar{\tilde{q}}_j$. Note that $t=(p_1-k_1)^2$ where the four momenta are chosen as indicated in parentheses: $q_i(p_1)+q_j(p_2)\to\tilde{q}_i(k_1)+\tilde{q}_j(k_2)$. Note that we disagree with ref. [11] on this point, as scalar quarks of different flavors are distinguishable in principle (see the discussion at the end of appendix B).

If $i=j$, then,

$$|\mathfrak{M}(qq\to\tilde{q}\tilde{q})|^2_{\text{ave}} = \tfrac{4}{9}g_s^4\left[k(t,u)+k(u,t)-\frac{2M_{\tilde{g}}^2 s}{3\left(t-M_{\tilde{g}}^2\right)\left(u-M_{\tilde{g}}^2\right)}\right], \quad \text{(A.10)}$$

where $k(t,u)$ is defined in eq. (A.9) and we have summed over $\tilde{q}_L$ and $\tilde{q}_R$. One subtlety here is the question of identical particles in the final state. Indeed, we must explicitly insert a factor of $\frac{1}{2}$ when computing the total cross-section. Since we do not include this factor of $\frac{1}{2}$ in our expressions for the squared matrix element, then we must define:

$$|\tilde{\mathfrak{M}}(qq\to\tilde{q}\tilde{q})|^2 = |\tilde{\mathfrak{M}}(qq\to\tilde{q}_L\tilde{q}_L)|^2 + |\tilde{\mathfrak{M}}(qq\to\tilde{q}_R\tilde{q}_R)|^2 + 2|\tilde{\mathfrak{M}}(qq\to\tilde{q}_L\tilde{q}_R)|^2. \quad \text{(A.11)}$$

The factor of 2 above accounts for $\tilde{q}_L\tilde{q}_R+\tilde{q}_R\tilde{q}_L$. (If we had used the convention where the factor of $\frac{1}{2}$ does appear in the squared matrix element when final state scalar quarks are identical, then no factor of 2 would be required in eq. (A.11). For further details, see appendix E.4 of ref. [5].)

(iii) $q_i\bar{q}_j\to\tilde{q}_k\bar{\tilde{q}}_\ell$ (fig. 11b). If $i\neq j$, then eqs. (A.8) and (A.9) apply here as well. If $i=j$ and $k=l$, then an additional Feynman graph is allowed (see fig. 11b) and we find:

$$|\mathfrak{M}(q\bar{q}\to\tilde{q}\bar{\tilde{q}})|^2_{\text{ave}} = \tfrac{4}{9}g_s^4\left[k(t,u)+\frac{n_f}{2s^2}\left[s\left(s-4M_{\tilde{q}}^2\right)-(u-t)^2\right]\right.$$
$$\left.+\frac{\left(M_{\tilde{q}}^2-t\right)(u-t)+s\left(M_{\tilde{q}}^2+t\right)}{3s\left(t-M_{\tilde{g}}^2\right)}\right]. \quad \text{(A.12)}$$

(iv) Scalar-quark production via W and Z decay (fig. 12). In the above formulas, we have neglected the contributions due to the exchange of a real or virtual W or Z. Consider the effects of the graphs shown in fig. 12. We make use of the following Feynman rules:

$$V_{q_i\bar{q}_j}: \quad -\tfrac{1}{2}ig\gamma^\mu\left[g_L\left(\frac{1-\gamma_5}{2}\right)+g_R\left(\frac{1+\gamma_5}{2}\right)\right], \quad \text{(A.13)}$$

$$V_{\bar{q}_k\bar{\tilde{q}}_i}: \quad -\tfrac{1}{2}igg_Z(k_1-k_2)^\mu, \quad \text{(A.14)}$$

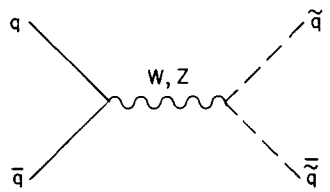

Fig. 12. Graph for the production of $\tilde{q}\bar{\tilde{q}}$ via W or Z bosons.

where V is a gauge boson and the four-momenta are defined as follows: $V \to \tilde{q}_k(k_1) + \bar{\tilde{q}}_l(k_2)$. The appropriate values of g_L and g_R for W and Z exchange may be obtained from figs. 71 and 72 of ref. [6]. For completeness, we summarize the results here:

$$g_L = \begin{cases} \sqrt{2}\,, & \text{for } Wq\bar{q} \text{ vertex} \\ \dfrac{2\left(T_3 - e_q \sin^2\theta_W\right)}{\cos\theta_W}\,, & \text{for } Zq\bar{q} \text{ vertex}, \end{cases} \tag{A.15}$$

$$g_R = \begin{cases} 0, & \text{for } Wq\bar{q} \text{ vertex} \\ \dfrac{-2e_q \sin^2\theta_W}{\cos\theta_W}\,, & \text{for } Zq\bar{q} \text{ vertex}, \end{cases} \tag{A.16}$$

$$g_Z = \begin{cases} g_L\,, & \text{for } V\tilde{q}_L\bar{\tilde{q}}_L \text{ vertex} \\ -g_R\,, & \text{for } Z\tilde{q}_R\bar{\tilde{q}}_R \text{ vertex}, \end{cases} \tag{A.17}$$

where $T_3 = +\frac{1}{2}, -\frac{1}{2}$ and $e_q = \frac{2}{3}, -\frac{1}{3}$ for the u and d quarks respectively. We then find:

$$\left|\bar{\mathfrak{M}}\left(q_i\bar{q}_j \to V \to \tilde{q}_k\bar{\tilde{q}}_l\right)\right|^2_{\text{ave}} = \frac{g^4 g_Z^2\left(g_L^2 + g_R^2\right)\left[s\left(s - 4M_{\tilde{q}}^2\right) - (t-u)^2\right]}{64\left[\left(s - m_V^2\right)^2 + \Gamma_V^2 m_V^2\right]}\,, \tag{A.18}$$

where we have allowed for the nonzero vector boson width, Γ_V. In eq. (A.18), we have *not* summed over different flavors of final state scalar-quarks; nor have we summed over $\tilde{q}_L$ and $\tilde{q}_R$. (We have taken two final-state scalar quarks to be degenerate in mass.) In principle, we must also compute the interference of fig. 12 with other diagrams contributing to $q_i\bar{q}_j \to \tilde{q}_k\bar{\tilde{q}}_l$. However, at the CERN collider, only the on-shell production of W and Z bosons can conceivably lead to appreciable scalar-quark production. In the limit that the vector boson is real, interference diagrams vanish and we may make use of eq. (A.18) along with a narrow width approximation, replacing the Breit-Wigner dominator by $(\pi/\Gamma_V m_V)\delta(s - m_V^2)$.

Equivalently, one can use a Monte Carlo routine to produce W and Z events, and then decay the W and Z into $\tilde{q}\bar{q}$. The relevant decay rate (for equal mass scalar quarks) is:

$$\frac{\Gamma(V \to \tilde{q}_k \bar{\tilde{q}}_l)}{\Gamma(V \to q_k \bar{q}_l)} = \frac{g_Z^2}{2(g_L^2 + g_R^2)} \left(1 - \frac{4M_{\tilde{q}}^2}{m_V^2}\right)^{3/2}. \tag{A.19}$$

Using eq. (A.17), it follows that

$$\frac{\Gamma(V \to \tilde{q}_L \bar{\tilde{q}}_L + \tilde{q}_R \bar{\tilde{q}}_R)}{\Gamma(V \to q\bar{q})} = \frac{1}{2} \left(1 - \frac{4M_{\tilde{q}}^2}{m_V^2}\right)^{3/2}. \tag{A.20}$$

A.4. $q\bar{q} \to \tilde{g}\tilde{\gamma}$ *(fig. 10c).*

$$|\tilde{\mathfrak{M}}(q\bar{q} \to \tilde{g}\tilde{\gamma})|_{\text{ave}}^2 = \frac{8g_s^2 e^2 e_q^2}{9} \left[\frac{(M_{\tilde{\gamma}}^2 - t)(M_{\tilde{g}}^2 - t)}{(M_{\tilde{q}}^2 - t)^2} + \frac{(M_{\tilde{\gamma}}^2 - u)(M_{\tilde{g}}^2 - u)}{(M_{\tilde{q}}^2 - u)^2} - \frac{2sM_{\tilde{g}}M_{\tilde{\gamma}}}{(M_{\tilde{q}}^2 - t)(M_{\tilde{q}}^2 - u)} \right], \tag{A.21}$$

where we have included both $\tilde{q}_L$ and $\tilde{q}_R$ exchange. Note that the two diagrams in fig. 10c differ by exchange of the final state fermions. Even though these fermions are not identical, Fermi-statistics requires that these two diagrams have a relative minus sign, leading to the sign of the interference term shown above.

A.5. $qg \to \tilde{q}\tilde{\gamma}$ *(fig. 11e).*

$$|\tilde{\mathfrak{M}}(qg \to \tilde{q}\tilde{\gamma})|_{\text{ave}}^2 = \frac{g_s^2 e^2 e_q^2}{3} \left[\frac{M_{\tilde{\gamma}}^2 - u}{s} + \frac{2M_{\tilde{q}}^2(t - M_{\tilde{\gamma}}^2)}{(t - M_{\tilde{g}}^2)^2} + \frac{2(t - M_{\tilde{\gamma}}^2)(M_{\tilde{q}}^2 - M_{\tilde{\gamma}}^2) - 2sM_{\tilde{\gamma}}^2}{s(t - M_{\tilde{q}}^2)} \right], \tag{A.22}$$

where we have added the results for $\tilde{q}_L$ and $\tilde{q}_R$ production.

A.6. $\tilde{g} \to q\bar{q}\tilde{\gamma}$ *(fig. 13).* We assume that $M_{\tilde{q}} > M_{\tilde{g}}$ so that the scalar-quark exchange is virtual. The squared amplitude for gluino decay may be obtained from eq. (A.21) by crossing symmetry. If one takes into account the different spin and color averages for the two processes: $\frac{1}{16}$ for $\tilde{g} \to q\bar{q}\tilde{\gamma}$ and $\frac{1}{36}$ for $q\bar{q} \to \tilde{g}\tilde{\gamma}$, one may

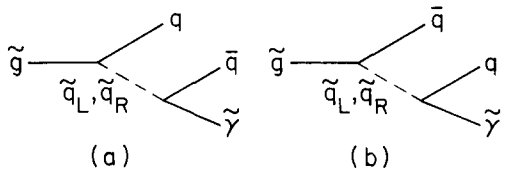

Fig. 13. Graphs for the gluino decay $\tilde{g} \to q\bar{q}\tilde{\gamma}$. The quarks q may run over all possible flavors such that the decay is kinematically allowed.

immediately write down:

$$|\tilde{\mathfrak{M}}(\tilde{g} \to q\bar{q}\tilde{\gamma})|^2_{\text{ave}} = 8g_s^2 e^2 e_q^2 \left[\frac{p \cdot k_1 k_2 \cdot k_3}{\left[(k_2+k_3)^2 - M_{\tilde{q}}^2\right]^2} + \frac{p \cdot k_2 k_1 \cdot k_3}{\left[(k_1+k_3)^2 - M_{\tilde{q}}^2\right]^2} + \frac{M_{\tilde{g}} M_{\tilde{\gamma}} k_1 \cdot k_2}{\left[(k_2+k_3)^2 - M_{\tilde{q}}^2\right]\left[(k_1+k_3)^2 - M_{\tilde{q}}^2\right]} \right], \quad \text{(A.23)}$$

where the four-momenta are defined by: $\tilde{g}(p) \to q(k_1) + \bar{q}(k_2) + \tilde{\gamma}(k_3)$. We have added both $\tilde{q}_L$ and $\tilde{q}_R$ exchanges and have assumed that these masses are equal.

If we take $M_{\tilde{\gamma}} = 0$, then we may easily integrate eq. (A.23) over phase space. The result is:

$$\Gamma(\tilde{g} \to q\bar{q}\tilde{\gamma}) = \frac{\alpha_s \alpha e_q^2 M_{\tilde{g}}}{4\pi} \left[3R - \tfrac{5}{2} + (3R-1)(R-1)\log\frac{R-1}{R} \right], \quad \text{(A.24a)}$$

where

$$R \equiv \frac{M_{\tilde{q}}^2}{M_{\tilde{g}}^2}. \quad \text{(A.24b)}$$

In the limit of infinite mass scalar-quarks ($R \to \infty$), we expand the logarithm and obtain:

$$\Gamma(\tilde{g} \to q\bar{q}\tilde{\gamma}) \xrightarrow[R \to \infty]{} \frac{\alpha_s \alpha e_q^2 M_{\tilde{g}}^5}{48\pi M_{\tilde{q}}^4}, \quad \text{(A.25)}$$

which is the well-known result [60].

A.7. $\tilde{g} \to q\tilde{q}$. We now assume that $M_{\tilde{q}} < M_{\tilde{g}}$ so that the emitted scalar-quark is real. If we compute the four possible final states: $q\bar{\tilde{q}}_L$, $q\bar{\tilde{q}}_R$, $\bar{q}\tilde{q}_L$ and $\bar{q}\tilde{q}_R$, the result upon adding is:

$$|\tilde{\mathfrak{M}}(\tilde{g} \to \bar{q}\tilde{q}_{L,R} + q\bar{\tilde{q}}_{L,R})|^2_{\text{ave}} = 4g_s^2 p \cdot k, \quad \text{(A.26)}$$

where p is the gluino four-momentum and k is the quark (or antiquark) four-momentum. It follows that the corresponding gluino width is:

$$\Gamma = \frac{\alpha_s\left(M_{\tilde{g}}^2 - M_{\tilde{q}}^2\right)^2}{2M_{\tilde{g}}^3}. \tag{A.27}$$

A.8. $\tilde{q} \to q\tilde{g}$. If $M_{\tilde{q}} > M_{\tilde{g}}$, then this decay is possible. For a fixed initial state,

$$|\tilde{\mathfrak{M}}(\tilde{q} \to q\tilde{g})|^2_{\text{ave}} = \tfrac{16}{3} g_s^2 p_1 \cdot p_2, \tag{A.28}$$

where p_1 and p_2 are the final state momenta. It follows that:

$$\Gamma(\tilde{q} \to q\tilde{g}) = \tfrac{2}{3}\alpha_s M_{\tilde{q}}\left(1 - \frac{M_{\tilde{g}}^2}{M_{\tilde{q}}^2}\right)^2. \tag{A.29}$$

A.9. $\tilde{q} \to q\tilde{\gamma}$. Using the same notation as in the last case

$$|\tilde{\mathfrak{M}}(\tilde{q} \to q\tilde{\gamma})|^2_{\text{ave}} = 4e^2 e_q^2 p_1 \cdot p_2, \tag{A.30}$$

implying that

$$\Gamma(\tilde{q} \to q\tilde{\gamma}) = \tfrac{1}{2}\alpha e_q^2 M_{\tilde{q}}\left(1 - \frac{M_{\tilde{g}}^2}{M_{\tilde{q}}^2}\right)^2. \tag{A.31}$$

Appendix B

AN EXAMPLE: SCALAR-QUARK PAIR PRODUCTION

We shall briefly discuss $\tilde{q}\tilde{q}$ production to illustrate some technicalities and to mention some simplifications which may occur. First, when scalar particles are produced (which subsequently decay), there is no need to compute the phase space for the n-body final state ($n > 2$). One simply computes the $2 \to 2$ subprocess. The final state scalar-quarks decay isotropically in their rest frames, and this is easily implemented in the Monte Carlo. Then, all we need to consider is

$$\sigma(p\bar{p} \to \tilde{q}\tilde{q} + X) = \sum_{a,b} \int dx_1\, dx_2\, f_a^p(x, Q^2) f_b^p(x_2, Q^2) \hat{\sigma}^{ab \to \tilde{q}\tilde{q}}(\hat{s}, \hat{t}, \hat{u}). \tag{B.1}$$

Let us use the results of appendix A. For simplicity, we neglect the contributions of

W and Z exchange. Let us denote:

$$|\tilde{\mathfrak{M}}(gg \to \tilde{q}\bar{\tilde{q}})|^2_{\text{ave}} = M_A(\hat{t}, \hat{u}), \tag{B.2}$$

$$|\tilde{\mathfrak{M}}(q_i q_j \to \tilde{q}_i \tilde{q}_j)|^2_{\text{ave}} = M_B(\hat{t}, \hat{u}), \qquad i \neq j, \tag{B.3}$$

$$|\tilde{\mathfrak{M}}(qq \to \tilde{q}\tilde{q})|^2_{\text{ave}} = M_C(\hat{t}, \hat{u}), \tag{B.4}$$

$$|\tilde{\mathfrak{M}}(q_i \bar{q}_i \to \tilde{q}_j \bar{\tilde{q}}_j)|^2_{\text{ave}} = M_D(\hat{t}, \hat{u}). \tag{B.5}$$

The relevant combinations of structure functions are given below:

$$P_1 = g(x_1)g(x_2), \tag{B.6}$$

$$P_2 = u(x_1)d(x_2) + \bar{u}(x_1)\bar{d}(x_2) + \bar{u}(x_1)d(x_2) + u(x_1)\bar{d}(x_2), \tag{B.7}$$

$$P_2' = d(x_1)u(x_2) + \bar{d}(x_1)\bar{u}(x_2) + d(x_1)\bar{u}(x_2) + \bar{d}(x_1)u(x_2), \tag{B.8}$$

$$P_3 = u(x_1)\bar{u}(x_2) + \bar{u}(x_1)u(x_2) + d(x_1)\bar{d}(x_2) + \bar{d}(x_1)d(x_2), \tag{B.9}$$

$$P_4 = u(x_1)u(x_2) + d(x_1)d(x_2), \tag{B.10}$$

$$P_4' = \bar{u}(x_1)\bar{u}(x_2) + \bar{d}(x_1)\bar{d}(x_2). \tag{B.11}$$

In this notation, $f_a^{\text{p}}(x) \equiv a(x)$ and $f_{\bar{a}}^{\text{p}}(x) = f_a^{\bar{\text{p}}} \equiv \bar{a}(x)$ where $a = \text{u}, \text{d}$ for the u and d quarks. The gluon distribution function is denoted by $g(x)$. We then may write eq. (B.1) as:

$$\sigma(p\bar{p} \to \tilde{q}\bar{\tilde{q}} + X)$$

$$= \int \text{dLIPS} \int dx_1\, dx_2 \{ P_1 M_A(\hat{t}, \hat{u}) + P_2 M_B(\hat{t}, \hat{u}) + P_2' M_B(\hat{u}, \hat{t})$$

$$+ \tfrac{1}{2} P_3 M_C(\hat{t}, \hat{u}) + P_4 M_D(\hat{t}, \hat{u}) + P_4' M_D(\hat{u}, \hat{t}) \}, \tag{B.12}$$

where dLIPS is the usual two-body Lorentz invariant phase space element. As discussed below eq. (A.10), an explicit factor of $\frac{1}{2}$ is required in the one case where the final state consists of identical scalar-quarks. Note that M_{B} and M_{D} are not $\hat{t} - \hat{u}$ symmetric; hence we must interchange $\hat{t}$ and $\hat{u}$ when we interchange x_1 and x_2 in going from $P_i \to P_i'$ $(i = 2, 4)$. This is the proper way to deal with final states consisting of distinguishable scalar quarks.

In more complicated processes, the procedure is similar except that in general we must construct the squared matrix element for a $2 \to n$ process $(n > 2)$, as shown in sect. 3. Then the integration dLIPS will refer to the appropriate n-body phase space element.

References

[1] G. Arnison, et al., CERN-EP/85-108 (1985);
L. Di Lella, invited talk given at the 1985 Lepton-photon conference, Kyoto, Japan, August 1985

[2] L. Susskind, Phys. Rev. D20 (1979) 2619;
G. 't Hooft, in Recent developments in gauge theories, Proc. NATO Advanced Summer Institute, Cargèse, 1979, ed. G. 't Hooft et al. (Plenum, New York, 1980) p. 135;
M. Veltman, Acta Phys. Polon. B12 (1981) 437;
C.H. Llewellyn Smith and G. G. Ross, Phys. Lett. 105B (1981) 38

[3] E. Witten, Nucl. Phys. B188 (1981) 513;
S. Dimopoulos and H. Georgi, Nucl. Phys. B193 (1981) 150;
N. Sakai, Z. Phys. C11 (1981) 153

[4] P. Fayet, in Quarks, leptons and supersymmetry, Proc. 17th Recontre de Moriond, ed. J. Tran Thanh Van (Editions Frontières, France, 1982) p. 483; in Proc. 21st Int. Conf. on High energy physics, ed. P. Petiau and M. Porneuf (Editions Frontieres, France, 1982) p. C3-673; in Proc. 14th summer school on particle physics, (Gif-sur-Yvette, France, 1982) p. 43

[5] D.V. Nanopoulos and A. Savoy-Navarro, Phys. Reports 105 (1984) 1

[6] H.E. Haber and G.L. Kane, Phys. Reports 117 (1985) 75

[7] J. Ellis, in Proc. Yukon Advanced Study Institute on the Quark structure of matter, ed. N. Isgur, G. Karl, and P.J. O'Donnell (World Scientific, Singapore, 1985) p. 256

[8] H.P. Nilles, Phys. Reports 110C (1984) 1;
P. Nath, R. Arnowitt and A.H. Chamseddine, Applied N = 1 supergravity, ICTP series in theoretical physics, vol. I (World Scientific, Singapore, 1985)

[9] E. Eichten, I. Hinchliffe, K. Lane and C. Quigg, Rev. Mod. Phys. 56 (1984) 579

[10] G.L. Kane and J.P. Leveille, Phys. Lett. 112B (1982) 227

[11] P.R. Harrison and C.H. Llewellyn Smith, Nucl. Phys. B213 (1983) 223; (E) B223 (1983) 542

[12] I. Antoniadis, L. Baulieu and F. Delduc, Z. Phys. C23 (1984) 119

[13] S. Dawson, E. Eichten, and C. Quigg, Phys. Rev. D31 (1985) 1581

[14] G. Arnison et al., Phys. Lett. 139B (1984) 115

[15] J. Ellis and H. Kowalski, Phys. Lett. 142B (1984) 441;
Nucl. Phys. B246 (1984) 189; Phys. Lett. 157B (1985) 437

[16] J. Ellis, and H. Kowalski, Nucl. Phys. B259 (1985) 109

[17] E. Reya and D.P. Roy, Phys. Rev. Lett. 51 (1983) 867 (E) 51 (1983) 1307; Phys. Rev. Lett. 53 (1984) 881; Phys. Lett. 141B (1984) 442; Phys. Rev. D32 (1985) 645; Dortmund preprint DO-TH 85/23 (1985);
V. Barger, K. Hagiwara and J. Woodside, Phys. Rev. Lett. 53 (1984) 641;
V. Barger, K. Hagiwara and W.-Y. Keung, Phys. Lett. 145B (1984) 147;
V. Barger, K. Hagiwara, W.-Y. Keung and J. Woodside, Phys. Rev. D31 (1985) 528; D32 (1985) 806;
A.R. Allan, E.W.N. Glover and A.D. Martin, Phys. Lett. 146B (1984) 247;
A.R. Allan, E.W.N. Glover, and S.L. Grayson, Nucl. Phys. B259 (1985) 77;
N.D. Tracas and S.D.P. Vlassopulos, Phys. Lett. 149B (1984) 253;
X.N. Maintas and S.D.P. Vlassopulos, Phys. Rev. D32 (1985) 604;
F. Delduc, H. Navelet, R. Peschanski and C. Savoy, Phys. Lett. 155B (1985) 173

[18] V. Barger, S. Jacobs, J. Woodside and K. Hagiwara, Wisconsin preprint MAD/PH/232 (1985)

[19] R.M. Barnett, H.E. Haber, and G.L. Kane, Phys. Rev. Lett. 54 (1985) 1983

[20] M.J. Herrero, L.E. Ibanez, C. Lopez and F.J. Yndurain, Phys. Lett. 132B (1983) 199; 145B (1984) 430

[21] A. De Rújula and R. Petronzio, Nucl. Phys. B261 (1985) 587

[22] G. Altarelli, B. Mele and S. Petrarca, Univ. La Spirenza (Rome), 1985

[23] J. Rohlf, invited talk at the 1985 Division of particles and fields conf., Eugene, Oregon, August 1985;
C. Rubbia, invited talk at the 1985 Lepton-photon conf., Kyoto, Japan, August 1985

[24] P. Fayet, Phys. Lett. 69B (1977) 489;
G. Farrar and P. Fayet, Phys. Lett. 76B (1978) 575

[25] P. Fayet, Phys. Lett. 86B (1979) 272

[26] J. Ellis and G.G. Ross, Phys. Lett. 117B (1982) 397

[27] H.E. Haber, G.L. Kane and M. Quiros, University of Michigan preprint UM TH 85-8; Phys. Lett. 160B (1985) 297
[28] H. Komatsu and J. Kubo, Phys. Lett. 157B (1985) 90
[29] C.S. Aulakh and R.N. Mohapatra, Phys. Lett. 119B (1982) 136; 121B (1983) 147;
L.J. Hall and M. Suzuki, Nucl. Phys. B231 (1984) 419;
J. Ellis, G. Gelmini, C. Jarlskog, G.G. Ross and J.W.F. Valle, Phys. Lett. 150B (1985) 142;
G.G. Ross and J.W.F. Valle, Phys. Lett. 151B (1985) 375
[30] S. Dawson, Nucl. Phys. B261 (1985) 297
[31] J. Ellis and S. Rudaz, Phys. Lett. 128B (1983) 248
[32] A.H. Chamseddine, R. Arnowitt and P. Nath, Phys. Rev. Lett. 49 (1982) 970;
S. Weinberg, Phys. Rev. Lett. 50 (1983) 387;
P. Fayet, Phys. Lett. 125B (1983) 178
[33] J.M. Frere and G.L. Kane, Nucl. Phys. B223 (1983) 331;
J. Ellis, J.S. Hagelin, D.V. Nanopoulos and M. Srednicki, Phys. Lett. 127B (1983) 233;
V. Barger, R.W. Robinett, W.Y. Keung and R.J.N. Phillips, Phys. Lett. 131B (1983) 372
[34] A.H. Chamseddine, P. Nath and R. Arnowitt, Northeastern preprint NUB #2681 (1985)
[35] W. Bartel et al., Phys. Lett. 146B (1984) 126; 155B (1985) 288; DESY 85-060 (1985);
B. Adeva et al. Phys. Rev. Lett. 53 (1984) 1806;
G.J. Feldman, et al., Phys. Rev. Lett. 54 (1985) 2289;
W. Ash et al., Phys. Rev. Lett. 54 (1985) 2477;
C. Akerlof et al., Phys. Lett. 156B (1985) 271;
H.J. Behrend et al., Phys. Lett. 161B (1985) 182
[36] F. Herzog and Z. Kunszt, Phys. Lett. 157B (1985) 430
[37] G. Sterman and S. Weinberg, Phys. Rev. Lett. 39 (1977) 1436
[38] F. Bergsma et al., Phys. Lett. 121B (1983) 429;
R.C. Ball et al., Phys. Rev. Lett. 53 (1984) 1314
[39] A.M. Cooper-Sarkar et al., Phys. Lett. 160B (1985) 212
[40] B.A. Campbell, J. Ellis and S. Rudaz, Nucl. Phys. B198 (1982) 1;
I. Antoniadis, C. Kounnas and R. Lacaze, Nucl. Phys. B211 (1983) 216;
C. Kounnas and D.A. Ross, Nucl. Phys. B214 (1983) 317;
S.K. Jones and C.H. Llewellyn Smith, Nucl. Phys. B217 (1983) 145;
M.J. Herrero, C. Lopez and F.J. Yndurain, Nucl. Phys. B244 (1984) 207
[41] G. Altarelli and G. Parisi, Nucl. Phys. B126 (1977) 285
[42] M. Mohammadi, CERN-EP/85-52 (1985), presented at the Conf. on Collider physics at ultra high energies, Aspen, Colorado, January 1985
[43] C. Peterson, D. Schlatter, I. Schmidt and P.M. Zerwas, Phys. Rev. D27 (1983) 105
[44] G. Arnison et al., CERN-EP/82-122 (1982)
[45] G. Arnison et al., Phys. Lett. 132B (1983) 214;
J. Sass, in Antiproton proton physics and the W discovery, Proc. Int. Colloquium of the CNRS, Third Moriond Workshop, March 1983, ed. J. Tran Thanh Van (Editions Frontières, France, 1983) p. 295
[46] P. Darriulat, invited lectures at the 13th SLAC Summer Institute on Particle physics, July 1985
[47] T. Gottschalk, F. Paige and T. Sjostrand, invited talks at the Supercollider physics Topical Conference, Eugene, Oregon, August 1985
[48] A. Honma and W. Kozanecki, private communication
[49] A. Honma, private communication
[50] S.D. Ellis, R. Kleiss and W.J. Stirling, Phys. Lett. 158B (1985) 341; CERN-TH-4307/85
[51] L. Alvarez-Gaumé, J. Polchinski, and M. Wise, Nucl. Phys. B221 (1983) 495;
J. Ellis, J. Hagelin, D.V. Nanopoulos and K. Tamvakis, Phys. Lett. 125B (1983) 275;
M. Claudson, L. Hall and I. Hinchliffe, Nucl. Phys. B228 (1983) 501;
S. Jones and G.G. Ross, Phys. Lett. 135B (1984) 69
[52] L. Ibanez and C. Lopez, Phys. Lett. 126B (1983) 54; Nucl. Phys. B228 (1983) 501
[53] C. Kounnas, A.B. Lahanas, D.V. Nanopoulos and M. Quiros, Phys. Lett. 132B (1983) 95; Nucl. Phys. B236 (1984) 438
[54] G. Arnison et al., Phys. Lett. 147B (1984) 493

[55] H. Goldberg, Phys. Rev. Lett. 50 (1983) 1419
[56] J. Ellis, J.S. Hagelin, D.V. Nanopoulos, K. Olive and M. Srednicki, Nucl. Phys. B238 (1984) 453
[57] J. Ellis and M. Sher, Phys. Lett. 148B (1984) 309;
L.J. Hall, and J. Polchinski, Phys. Lett. 152B (1985) 335;
M. Gluck, E. Reya and D.P. Roy, Phys. Lett. 155B (1985) 284;
S. Nandi, Phys. Rev. Lett. 54 (1985) 2493;
L. Ibanez, C. Lopez and C. Munoz, Nucl. Phys. B256 (1985) 252;
K. Enqvist, D.V. Nanopoulos and A.B. Lahanas, Phys. Lett. 155B (1985) 83;
J. Ellis, J.S. Hagelin and D.V. Nanopoulos, Phys. Lett. 159B (1985) 26
[58] W. Bartel, et al., Phys. Lett. 139B (1984) 327
[59] H.M. Georgi, S.L. Glashow, M.E. Machacek and D.V. Nanopoulos, Ann. of Phys. (NY) 114 (1978) 273
[60] H.E. Haber and G.L. Kane, Nucl. Phys. B232 (1984) 333